Interpretation of Large Ionization Bursts Observed at High Altitudes in High Pressure Chambers under Thick Shields

Thesis by
Erdal İsmet İnönü

In Partial Fulfillment of the Requirements
for the Degree of
Doctor of Philosophy

California Institute of Technology
Pasadena, California
1952

Acknowledgements

It is a great pleasure to thank Professor R. F. Christy for proposing this problem and for guiding me throughout with many important suggestions as well as with constant encouragement. I am much indebted to Professor H. V. Neher for most helpful discussions on his burst experiments and on the primary cosmic ray spectrum.

Finally my thanks go to Miss Jeanne Antz for drawing the figures.

Abstract

An attempt is made to explain the ionization bursts containing 400 - 1600 particles observed at high altitudes in high pressure chambers heavily shielded with lead, in terms of short-lived neutral mesons produced by primary protons colliding with shield nuclei; neutral mesons instantly decay into photons which initiate electron cascades in the shield resulting in an ionization burst inside the chamber. The primary interaction is treated by means of a simple model for multiple meson production which assumes constant cross section, complete inelasticity and constant multiplicity throughout the energy region $10^{11} - 10^{13}$ ev; 1/3 of the primary energy is assumed to go into neutral mesons.

The contribution of the soft component of high energy air showers is estimated and found to be negligible at all altitudes. An analysis of burst data obtained by Neher and Biehl at three altitudes (307 gm, 616 gm, 1030 gm) then shows that the majority of high altitude bursts can be explained by neutral mesons produced in the primary encounter; but not a negligible fraction must be attributed to secondary collisions. From the data of Neher-Biehl and Fahy mean free paths of 185 $\mp$ 20 gm in air and 355 $\mp$ 55 gm in lead are deduced.

Table of Contents

LIST OF FIGURES

Figure

LIST OF FIGURES (continued)

Figure

Introduction

Large ionization bursts observed in heavily shielded high pressure chambers yield information on the interaction with matter of the high energy part of cosmic rays. The majority of such bursts are due to many fast electrons and positrons resulting from the cascade multiplication of a few soft rays in the material above the chamber. There are three main types of events that generate these soft rays.

(a) μ-mesons can produce fast electrons (knock-on) in their elastic collisions with atomic electrons or can emit hard γ-rays in the electric field of a nucleus (bremsstrahlung).

(b) High energy protons of the primary radiation can interact with the nuclei of the shield and produce neutral mesons which instantly decay into γ-rays.

(c) Air showers with sufficiently high energies can produce appreciable bursts either by penetrating the shield with their soft component or by generating decay photons in the shield through nuclear interaction of their penetrating component.

The contribution of μ-mesons was first calculated by Christy and Kusaka in 1940 (Ref. 1) and the results were successfully applied to the interpretation of the sea level bursts observed by Schein and Gill (Ref. 2).

Although more than enough to account for the sea level bursts (owing to a too low value for μ-meson mass), this effect could not explain the high altitude bursts of Schein and Gill and later of Schein and Lapp (Ref. 3) and Lapp (Ref. 4). The rise of the burst frequency with altitude is more rapid than the absorption of the μ-mesons in the atmosphere. The suggestion of Schein and Gill that high altitude bursts could be due to giant extensive showers was felt to be unsatisfactory after it was shown by Lapp that at sea level only a few percent of the bursts were coincident with air showers and it was difficult to see how the frequency of such giant showers could increase with altitude as rapidly as the burst frequency. A possible explanation in terms of primary protons was suggested by Bridge, Rossi and Williams (Ref. 5) and again by Bridge, Hazen and Rossi (Ref. 6) on the basis of coincidence experments made by means of a heavily shielded pulse ionization chamber and a bank of G-M tubes. After the discovery at Berkeley of short-lived neutral mesons that decay into γ-rays (Ref. 7, 8) it became evident that such was a significant process in producing bursts.

In the first part of this thesis the frequency of bursts due to the interaction of primary protons with the nuclei of the shield (shield bursts) is calculated on the basis of a simple model for multiple meson production.

In the second part the contribution of the soft component of air showers (air bursts) is estimated using the same model. The results are applied in the third part to the analysis of available burst data including some obtained by Neher and Biehl in airplane flights at 30,000 feet.

Part I. Shield Bursts

1. Model for multiple meson production

The bursts that interest us contain more than 300 - 2000 particles and can be initiated by protons in the energy region of 10^{11} - 10^{12} ev. Our knowledge of the interaction between nuclei at such energies is very scanty at present. So far there has been obtained only a few photographs showing such collisions between an impinging proton or α-particle and a nucleus at rest (Ref. 9 - 11). Their general characteristics seem to be the following:

(a) After the collision several minimum ionization tracks, presumed to be π-mesons both positively and negatively charged, emerge in the forward direction. These tracks are divided into two distinct cones; a very narrow core directly in line with the incoming particle and a diffuse cone around it. At even wider angles a few non-relativistic heavy particles are seen, some of which emerge actually in the backward direction.

(b) The number of mesons in the two cones vary from

one photograph to another, but it does not seem to change as rapidly as the primary energy. Thus it appears to favor Fermi's statistical theory (Ref. 12) according to which the multiplicity depends on the fourth root of the energy of the impinging nucleon in the laboratory system. We cannot use this theory for our calculations directly since it describes a collision between two nucleons whereas we are interested in collisions between a nucleon and a lead nucleus. In such a case plural production effects are certainly significant and besides increasing the multiplicities given by Fermi's pure multiple production theory, introduce large fluctuations in these figures (Ref. 13). There is no complete theory of plural-multiple production at present.

For our purposes, however, because of the integrating effect of the cascade process, a simplified model that assumes a constant multiplicity throughout the energy region of interest should suffice. As will be seen more clearly later, the important factor in determining the burst frequency is the amount of energy that goes into γ-rays starting the cascades and not so much the actual mechanism of this transformation.

In choosing our model we have copied the R-star obtained by Bradt, Peters and Kaplon (Ref. 9 and 14) which is attributed to a collision of a primary α-particle of energy around $10^{12} - 10^{13}$ ev with a heavy nucleus of the

emulsion (Ag or Br). The collision gave rise to a very narrow shower of 23 relativistic singly charged particles together with a diffuse shower of 33 relativistic particles. Assuming that all these particles are charged π-mesons, that the number of unseen neutral mesons is one half the number of charged mesons, and that all four nucleons of the α-particle contribute equally to the shower, we have 21 mesons produced per incoming nucleon of energy around $2.5 \times 10^{11} - 2.5 \times 10^{12}$ev, 9 of them in the narrow core and 12 in the diffuse cone. We now simplify the angular distribution by assuming that all nine particles of the core make equal angles with the axis (the direction of the incoming nucleon) and consequently have equal energies; and that similarly all twelve particles of the diffuse shower diverge on the same cone with equal energies. Making the additional assumption that particles in both cones have the same transverse momentum we obtain the following relation

$$p_w \sin\theta_w = p_n \sin\theta_n \qquad (1.1)$$

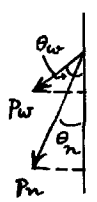

where p_w , p_n , θ_w , θ_n are respectively the momenta and polar angles of the particles in the wide and narrow cones, as shown in the figure. Or since all the particles are highly relativistic we can replace momenta by energies γ_w ,

γ_n and obtain

$$\gamma_w \sin\theta_w = \gamma_n \sin\theta_n \tag{1.2}$$

from which

$$\frac{\gamma_n}{\gamma_w} = \frac{\sin\theta_w}{\sin\theta_n} = \alpha \tag{1.3}$$

Let E be the total energy of the incoming nucleon, then neglecting the small fraction carried away by low energy heavy particles, we have

$$E = 9\gamma_n + 12\gamma_w \tag{1.4}$$

The percentages of energy in the narrow and wide cones are respectively,

$$x = \frac{9\gamma_n}{9\gamma_n + 12\gamma_w} = \frac{9\alpha}{9\alpha+12} \tag{1.5}$$

$$1-x = \frac{12\gamma_w}{9\gamma_n + 12\gamma_w} = \frac{12}{9\alpha+12}$$

Since 1/3 of the mesons are neutral and they decay into 2 γ-rays each we obtain 6 photons in the narrow cone and 8 photons in the wide one. The energy of a photon in the narrow cone is given by

$$E_n = \frac{\gamma_n}{2} = \frac{xE}{18} = \frac{\alpha E}{2(9\alpha+12)} \tag{1.6}$$

and in the wide cone by

$$E_w = \frac{\gamma_w}{2} = \frac{(1-x)E}{24} = \frac{E}{2(9\alpha+12)} \qquad (1.7)$$

For the polar angle θ_n we take the median value of the observed angular distribution in the core of the R-star, i.e. the value around which there are an equal number of mesons on both sides, which is $1^{\circ}.5$. The value for θ_w is similarly derived from the R-star as 10°, but for convenience in our subsequent shower calculations we take $\theta_w = 11^{\circ}\ 20'$. With these values (1.3), (1.5), (1.6), (1.7) yield

$$\alpha = 7.5$$

$$x = 0.85$$

$$E_n = \frac{E}{21.2} \quad , \qquad E_w = \frac{E}{160}$$

Therefore, for our purposes the collision of an incoming proton of energy E with a lead nucleus results in the production of 6 photons of energy $\frac{E}{21.2}$ and 8 photons of energy $\frac{E}{160}$ which initiate in the shield 14 cascades jointly responsible for the bursts.

Several remarks may be made here:

(a) In computing the frequency of shield bursts we can neglect the initial angular divergence of the showers in the wide cone. The wide showers contribute only 1/7 of the total burst particles; also near the edge of the chamber the showers that escape due to obliqueness are nearly compen-

sated by showers that enter the chamber obliquely, as the shield completely surrounds the chamber.

(b) The decay photons are emitted in the direction of motion of the neutral meson simply because of its high energy and the resulting relativistic transformation from center of mass system to laboratory system. Assuming isotropic emission of γ-rays in the center of mass system in which the neutral meson is at rest, one obtains in the laboratory system an intensity distribution proportional to $\frac{1}{\gamma^2 (1-\beta\cos\theta)^2}$, where γ is the energy of the neutral meson in terms of its rest energy, β is its velocity in terms of velocity of light (also $\gamma = \frac{1}{\sqrt{1-\beta^2}}$) and θ is the laboratory angle of emission of the photons. For a proton of 100 Bev energy, which is about the minimum energy for obtaining bursts with more than 400 particles in the Neher ionization chamber, we have for the mesons in the narrow cone $\gamma \sim 70$ and for the ones in the wide cone $\gamma \sim 10$. A polar diagram showi the intensity distribution for $\gamma = 10$ is reproduced bel The distribution for $\gamma = 70$ is even more strongly peake

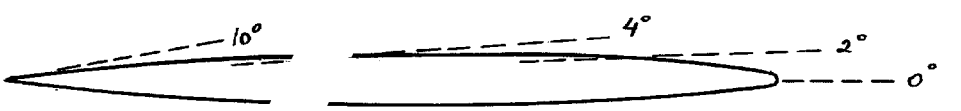

(c) The life-time of the neutral meson is estimated to be less than 10^{-13} sec (Ref. 9,15). If we take it as 10^{-14} sec, a neutral meson of energy $\gamma = 100$ will travel $3 \times 10^{10} \times 10^{-14} \times 100 = 0.03$ cm before it decays; a negligible distance compared to the radiation unit in lead which is of the order of cm. Thus we can safely assume that all the showers start at the collision point.

(d) The assumption that one-third of the total energy of the primary proton goes into neutral mesons may be harder to justify. The observations of Carlson et al (Ref. 15) which presumably refer to collisions of primary nucleons of energy 1 - 10 Bev show that in fact on the average one neutral meson is produced for every two charged π-mesons. However it is not clear that when we go to the higher range 100 - 1000 Bev the appearance of new particles (such as the V-mesons) will not change this balance significantly. The statistical theory of Fermi predicts that in nucleon-nucleon collisions the production of nucleon-antinucleon pairs will be appreciable only for energies higher than $\sim$ 1000 Bev. The effects of plural production may perhaps be expected to push this limit even higher. So that as far as nucleon-antinucleon pairs are concerned we feel confident that the assumed energy balance will be valid. The final justification would lie in its success as a working hypothesis.

(e) We have neglected the few heavy particles that come out of the collision. In the R-star the total energy carried by such particles is only about 1% of the primary energy. Furthermore they are emitted nearly isotropically in the laboratory system. Thus only one or two heavily ionizing particles will reach the chamber together with the electron cascades and in a high pressure chamber their ionization will not appreciably increase the burst size.

(f) The charged π-mesons in the narrow cone could interact with lead nuclei a second time before reaching the chamber and thus produce new showers that would increase the size of the observed bursts. We shall estimate this effect in section 3.d.

(g) In analyzing the R-star the assumption of equal transverse momenta for all mesons was made to obtain the relative energies of the narrow and wide cones. Whatever the merits of this special picture, since the apparent angular distribution is so sharply peaked, it is reasonable to expect that the actual energy division will not be significantly different. For instance if one takes the view that only the narrow core is produced in the initial encounter and the diffuse shower is produced in secondary and tertiary collisions of the nucleons of the incoming α-particle and the target nucleons, then assuming that the core mesons are

emitted in the center of mass system monoenergetically and with a $\cos^2 \theta$ distribution (which is one of the alternatives favored by Bradt et al) one finds that 86% of the incoming energy goes into the narrow cone.

2. Remarks on Shower Theory

The development of the photon-initiated cascades will be described in terms of standard shower theory which treats the longitudinal development of the shower independently from its lateral spread. Specifically we shall use Snyder's recent figures for the total number of expected particles at any point along the development of the shower (Ref. 16). Two objections have to be met in this connection:

First, the usual argument for neglecting the lateral spread in computing the number of particles along the shower axis, that the deviations due to multiple Coulomb scattering are small is not valid for showers in heavy elements such as lead. According to calculations of Nordheim and Roberg (Ref. 17) the average deflection of shower particles with critical energy is around 66° in lead. Thus a shower in lead, at a point near or after its maximum development, looks almost isotropic. Fortunately however the effect of this heavy scattering on the shape of the cascade curve (total number of particles as function of thickness traversed) is small due to the fact that the

position and magnitude of the maximum are mainly determined by high energy particles. In fact Belenky has shown that the inclusion of scattering in the diffusion equations with neglect of ionization loss, changes the position and magnitude of the maximum only by about 5% for an initiating electron of 0.5 Bev (Ref. 18). The showers that we are interested in start with even higher energies and consequently should be even less affected by scattering in their development.

Scattering also introduces large boundary effects which would be very hard to account for theoretically but which can be largely eliminated experimentally by completely surrounding the measuring apparatus with lead. As discussed by Christy and Kusaka (Ref. 1), for the comparison of theoretical burst calculations with experiments it is essential that this requirement be met. A spherical ionization chamber surrounded by a spherical shield is an ideal arrangement. Since our treatment applies to such an arrangement we feel justified in neglecting scattering in the development of our showers.

Secondly, in his treatment of the elementary processes of bremsstrahlung and pair creation, Snyder uses the so-called "completely screened" cross sections which are the asymptotic forms valid for very high energy particles. In

this way too high a probability is assigned to the processes (especially pair creation) associated with the lower energy particles in the shower. The difference was thought to be insignificant on light materials such as air or water, but important in heavy materials like lead because of the approximate $1/Z$ dependence of the critical energy in consequence of which the average energy of a shower particle at the maximum development is about 10 times smaller in lead compared to air. (For instance, the total pair cross section for a photon decreases by a factor of 3 by going from the high initial energies of the shower to the critical energy of $\sim$ 10 Mev.) A recent investigation by Bernstein (Ref. 19) shows that even for air there is an appreciable correction to be made to Snyder's "completely screened" figures. By means of a perturbation method he was able to find the effect of using a better approximation to the accurate Bethe-Heitler cross sections (Ref. 20) rather than the "completely screened" one. The result is, first, a decrease in the height of the shower maximum together with a slight shift to larger depths and, second, a decrease in the average number of electrons present at small depths with a corresponding increase at large depths. For our purposes these features can be represented in the first approximation as an increase in both the critical energy β

and the shower unit X_o. Since the height of the maximum is inversely proportional to the critical energy, the increase in β is determined by the required decrease in the maximum as was already pointed out by Christy and Kusaka. Similarly, the required increase in the size of the shower unit may be deduced from the shift in the position of the maximum. In this way one might be able to represent with sufficient accuracy the development of the showers near their maximum, which is the important region for burst calculations.

We can not make direct use of Bernstein's numerical results to determine β and X_o for lead. His perturbation method gives quantitatively accurate results only for light elements and breaks down for lead. However, considering the general trend of his plots for air and iron it is reasonable to expect for β an increase from the conventional value of 7 Mev to something around 10 Mev (for an initial energy given by $\ln \frac{E}{\beta} = 8$ in fig. 2 of Ref. 19) with a smaller increase for X_o. This is in agreement with Belenky's earlier results for lead. (Ref. 24) By means of a slightly approximate method of solving the diffusion equations, Belenky has estimated for several initial energies the effect of using the exact cross section for pair production on the position and height of

the maximum in lead. Denoting by t_m the position of the maximum and by N_m the number of particles at the maximum he obtains

$$t_m = K_1 \left(\frac{E_0}{\beta}\right) \ln \left(\frac{E_0}{\beta}\right) X_0$$

$$N_m = \frac{K_2 \left(\frac{E_0}{\beta}\right)}{\sqrt{\ln \left(\frac{E_0}{\beta}\right)}} \cdot \frac{E_0}{\beta}$$

with the following Table 1 for the values of K_1, K_2 for several initial energies E_0.

Table 1

E_0 in Bev	K_1	K_2
0.5	1.4	0.172
1	1.33	0.180
10	1.23	0.200

In the "completely screened" approximation K_1 and K_2 are constants and have the usual values of $K_1 = 0.96$, $K_2 = 0.3$. Neglecting the small change in the logarithmic factor and using $X_0 = 5.83$ gm/cm^2, $\beta = 7$ Mev as the conventional values we obtain from Belenky's figures the following Table 2 for the corrected values of β and X_0.

Table 2

E_0 in Bev	β in Mev	X_0 in gm/cm^2
0.5	12.2	8.5
1	11.7	8.1
10	10.5	7.5
100	9.6	7.1

An experimental verification for the variation in X_0 is provided by the recent experiments with the X-ray beam of the 322 Mev synchrotron at Berkeley. From an analysis of shower curves obtained by Blocker et al (Ref. 21) W. Aron deduced the value of 8.8 gm/cm^2 for the shower unit in lead. Subsequently Crowe and Hayward studied experimentally the differential energy spectrum of electrons at the maximum of the shower in lead and obtained good agreement with theory (as presented essentially by Snyder) using $X_0 = 8.8$ gm/cm^2. This is in satisfactory agreement with Belenky's value of $X_0 = 8.5$ gm/cm^2 for $E_0 = 500$ Mev. A check on the value of β can not be obtained from these experiments because of the unknown normalization factors. On the theoretical side we might note that recently Messel (Ref. 25) pointed out that the number of particles at the maximum in lead as given by Snyder and tentatively corrected by Bernstein comes very close to that given earlier by Bhabha and Chakrabarty (Ref. 26) who obtained this low value by letting some of the shower energy escape in the form of low energy quanta incapable of creating any pairs. Thus it appears that according to all estimates Snyder's solution together with Belenky's corrections represents the development of the showers near the maximum sufficiently accurately for

our purposes.

The shield bursts are effectively produced by photons with energies of the order of 10 Bev. Hence in computing such bursts we may use the values for $E_0 = 10$ Bev as given in Table 2 and neglect the small variation with burst size. Similarly in dealing with the air bursts where the relevant energies are higher by a factor of 10, the values for $E_0 = 100$ Bev may be used. However there is one more correction to be applied to β . In the original value of 7 Mev as ionization loss in 5.9 gm/cm^2 the polarization of the medium was not taken into account. According to the latest calculations by Halpern and Hall (Ref. 23) the reduction in loss due to polarization in lead is for an electron of 10 Mev, $\Delta = 0.046$ Mev per gm/cm^2 and for a shower unit (7.5 gm/cm^2) it is 0.3 Mev. Thus we obtain finally $\beta = 10.2$ Mev, $X_0 = 7.5$ gm/cm^2 for shield bursts and $\beta = 9.3$ Mev, $X_0 = 7.1$ gm/cm^2 for air bursts.

In all our work we shall be satisfied with the expected number of particles and shall not worry about the actual fluctuations that may occur around this average value. This may be justified by observing that our showers start their development already with 14 particles, so that even at the beginning where the fluctuations are usually preponderant they are smoothed out in this case by the

initial multiplicity.

3. Size-frequency distribution of shield bursts

(a) Analytical formulation. We are now going to derive the frequency of bursts containing more than S particles, produced under a given thickness α of lead. The reason for obtaining an integral size-frequency distribution rather than a differential one is both theoretical and experimental. Theoretically it is easier to derive such a distribution and experimentally one acquires more accuracy and better statistics by adding up all the bursts larger than a certain size. Let the differential spectrum of the primary cosmic radiation at the atmospheric depth t be f(E,t)dE particles per cm^2 sec sterad, its absorption mean free path in lead λ_A, and its collision mean free path in lead λ_c which may or may not be equal to λ_A ; both λ_A and λ_c will be assumed to be independent of energy. Unless otherwise stated, all lengths connected with the shield will be measured in terms of the shower unit in lead while all distances in air will be measured in terms of the shower unit in air. The average number of bursts that originate at a distance X and in a thickness dX of the shield and which are due to protons with energies between E and E + dE is given by

$$f(E,t)\,dE\; e^{-\frac{\alpha-X}{\lambda_A}}\; \frac{dX}{\lambda_c} \qquad \text{per } cm^2 \text{ sec sterad}$$

where X is measured in the direction opposite to that of the incoming beam. The number of particles contained in these bursts will depend on the initial proton energy E and on the remaining distance X in the shield over which the showers develop. For a sufficiently high initial energy there will be a definite distance in the shield in which if the proton makes a collision the resulting cascades will have more than S particles when they reach the ionization chamber. The limits of this burst range are shown in the figure below where the cascade curves starting at the two limit points and belonging to the same initial energy are represented schematically.

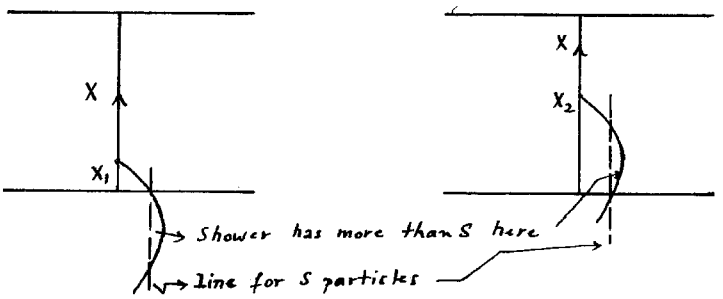

Thus the average number of bursts containing more than S particles will be obtained by integrating over the primary spectrum weighted according to the allowed burst range:

$$N(>S) = \int_{E_S}^{\infty} f(E,t)\, dE \int_{X_1(E)}^{X_2(E)} e^{-\frac{\alpha - X}{\lambda_A}} \frac{dX}{\lambda_e} \qquad (3.1)$$

where E_S is the proton energy that gives exactly S particles at the maximum of the showers and is therefore the minimum energy that can initiate bursts with more than S particles. Integrating over X one obtains

$$N(>S) = \int_{E_S}^{\infty} f(E,t)\, dE\; e^{-\frac{a}{\lambda_A}}\; \frac{\lambda_A}{\lambda_c}\left(e^{\frac{X_2(E)}{\lambda_A}} - e^{\frac{X_1(E)}{\lambda_A}} \right) \qquad (3.2)$$

As will be seen in the actual computations the burst range $\Delta X = X_2 - X_1$ is small compared to λ_A, so that one can use the following approximation to simplify the calculations:

$$e^{\frac{X_2}{\lambda_A}} - e^{\frac{X_1}{\lambda_A}} = e^{\frac{X_1}{\lambda_A}}\left(e^{\frac{\Delta X}{\lambda_A}} - 1 \right) \cong e^{\frac{X_1(E)}{\lambda_A}}\; \frac{\Delta X(E)}{\lambda_A} \qquad (3.3)$$

Since $X_1(E)$ is also small compared to λ_A, the exponential may be taken out of the energy integration by substituting an effective value for X_1, to be denoted by $\widetilde{X}_1(S)$. Thus:

$$N(>S) = \frac{e^{-\frac{a}{\lambda_A}}\; e^{\frac{\widetilde{X}_1(S)}{\lambda_A}}}{\lambda_c} \int_{E_S}^{\infty} f(E,t)\;\; \Delta X_S(E)\, dE \qquad (3.4)$$

per cm² sec sterad.

Following the general practice we shall assume for the vertical primary radiation a simple exponential absorption in the atmosphere with a constant mean free path t_A. Thus the form of the spectrum will remain unaltered throughout the atmosphere. This assumption is usually justified

by noting that because of the steepness of the energy spectrum the increase in the low energy particles due to the slowing down of the high energy ones is negligible and consequently a cross section for catastrophic collisions that does not depend on energy results in a uniform decrease in the number of particles at all energies. These considerations were recently quantitatively checked by Milford and Foldy (Ref. 27) and found to be quite valid. By assuming that a meson producing collision between two relativistic nucleons is completely inelastic and that the collision cross section is independent of energy they showed that an initial power law differential spectrum with an exponent of -3 will be absorbed exponentially throughout the atmosphere and without changing its form, provided we limit ourselves to energies higher than $\sim$ 50 Bev. We therefore assume for the vertical radiation a spectrum of the form

$$f(E,t)\,dE = \frac{P_0}{E^{n+1}}\, e^{-\frac{t}{t_A}}\, dE \qquad (3.5)$$

and we shall carry out calculations with n = 1.5 and n = 2.

The spherical ionization chamber receives rays coming from the whole upper hemisphere. Assuming that the primary radiation is hemispherically isotropic on top of the atmosphere we can readily integrate over angles and obtain the

Gross expression (Ref. 28) for the integrated intensity:

$$\int_0^{\frac{\pi}{2}} e^{-\frac{t \sec\theta}{t_A}} 2\pi \sin\theta \, d\theta$$

$$= 2\pi \left\{ e^{-\frac{t}{t_A}} - \frac{t}{t_A} \int_{t/t_A}^{\infty} \frac{e^{-u}}{u} du \right\} = 2\pi J(t/t_A) \qquad (3.6)$$

A plot of J(y) for the useful values of y will be found in fig. 19. Combining (3.5) and (3.6) with (3.4) one obtains

$$N(>S) = 2\pi \rho_0 J(t/t_A) \frac{e^{-\frac{a}{\lambda_A}} e^{\frac{\tilde{x}_1(S)}{\lambda_A}}}{\lambda_c} \int_{E_S}^{\infty} \frac{\Delta x_S(E)}{E^{n+1}} dE \qquad (3.7)$$

or substituting $E = 21.2\beta e^{\varepsilon}$ where β is the critical energy in lead and ε the new integration variable, one finds finally

$$N(>S) = \frac{2\pi \rho_0}{(21.2\beta)^n} J(t/t_A) \frac{e^{-\frac{a}{\lambda_A}} e^{\frac{\tilde{x}_1(S)}{\lambda_A}}}{\lambda_c} M(S) \quad \text{per cm}^2\text{.sec.} \qquad (3.8)$$

with the abbreviation $$M(S) = \int_{\varepsilon_S}^{\infty} \Delta x_S(\varepsilon) e^{-n\varepsilon} d\varepsilon \qquad (3.9)$$

(b) Evaluation of M(S). A graphical method is used to determine $\Delta x_S(\varepsilon)$ after which the integration is carried out numerically. In shower theory it is convenient to use for the energy variable $\varepsilon = \ln \frac{E}{\beta}$ where E is the initial energy; thus we have for the showers of the narrow and wide cones respectively $\varepsilon = \ln \frac{E}{21.2\beta}$ and $\varepsilon' = \ln \frac{E}{160\beta} = \varepsilon - 2$

(It was to obtain such a simple relation between ε and ε' that we took $11^0\ 20'$ for the angle of the wide cone instead of 10^0 as suggested by the R-star.) In figure 1 we have plotted cascade curves for several values of ε which are obtained by adding 6 showers of initial energy ε together with 8 showers of initial energy $\varepsilon - 2$. They give the expected number of particles $\tilde{N}$ at any distance u from the point of collision. From these plots the values of $\Delta x_s(\varepsilon)$ were derived for several values of ε and S, in the way indicated below schematically.

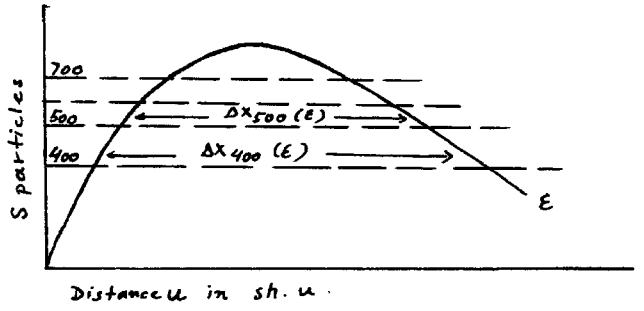

These values were in turn plotted to obtain the variation of $\Delta x_s(\varepsilon)$ for each S, as shown in fig. 2. The zeros of $\Delta x_s(\varepsilon)$ corresponding to the minimum values ε_s are taken from fig. 3 which represents the variation of $\tilde{N}_m$, the number of particles at the maximum of the total shower, with ε. Using the curves in fig. 2, M(S) was evaluated numerically for n = 1.5 and n = 2 by means of Simpson's rule with intervals of $\Delta\varepsilon = 0.1$. The results

for S = 400 - 1600 are listed below in Table 3 and plotted in fig. 4. The straight lines fitting the data in fig. 4 have slopes of -2.1 and 1.56 corresponding to n = 2.0 and n = 1.5 respectively. Therefore the size-frequency distribution of shield bursts must reflect the shape of the primary spectrum quite closely. Differences of ∓ 0.1 in the exponent are negligible owing to the low accuracy of data. Fig. 4 also shows the variation of the product $M(s) \cdot e^{\frac{\tilde{x}_1(s)}{\lambda_A}}$ for n = 2.0 where λ_A = 310 gm/cm^2 (See III 14) and $\tilde{x}_1(s)$ is taken from Table 2 (See 3 c); its slope -2.06 is even closer to the original slope.

Table 3

S	M(S) with n = 1.5	M(S) with n = 2.0
400	45 x 10^{-5}	141 x 10^{-7}
500	32	91
600	24	60
700	18	43
800	15	33
900	12	26
1000	10.5	21
1100	9.1	17
1200	8.0	14
1300	7.0	12
1400	6.3	10
1500	5.6	8.8
1600	5.0	7.6

The figures in Table 3 are computed by assuming a shield thickness of 13.45 shower units. However because the main contribution to the integral comes from a distance of only a few shower units, the actual value of M(S) is

insensitive to the shield thickness as long as the latter is larger than about 13 shower units. In fact we have computed M(1000) for $\alpha = 37.8$ and found it to be larger than that for $\alpha = 13.45$ by only 3%.

(c) Most probable energies and effective burst ranges for $n = 2$.

For estimating various corrections it is convenient to have approximate but unique values of the energy and burst range best suited to represent a given size burst. Following Christy and Kusaka we define for each S a most probable energy E_{max} given by the energy at the maximum of the integrand of M(S), and an effective burst range given by the relation

$$M(S) = \frac{1}{2}\,\eta\, e^{-2\varepsilon_{max}}$$

where $E_{max} = 21.2\,\beta\, e^{\varepsilon_{max}}$

We restrict ourselves to the case $n = 2.0$ as it seems to be closer to the actual value. In the first four columns of Table 4 we listed the figures for E_{max}, $\frac{E_{max}}{S}$ and η for bursts with S = 400 - 1600. E_{max} was determined by plotting the integrand of M(S) near its maximum for each S and consequently it has an uncertainty of about $\mp$ 0.01; this is responsible for the apparent non-uniform variation with S.

Table 4

S	ε_{max}	η	$\varepsilon_{max}/\beta S$	ε_{min}	$\tilde{x}_1(S)$
400	6.36	9.4	30.6	6.06	3.5
500	6.60	9.8	31.1	6.30	4.1
600	6.79	9.5	31.4	6.50	4.2
700	6.96	9.5	31.9	6.67	4.3
800	7.10	9.7	32.1	6.81	4.4
900	7.23	9.9	32.5	6.94	4.6
1000	7.34	9.9	32.7	7.05	4.7
1100	7.44	9.9	32.8	7.16	4.9
1200	7.53	9.7	32.9	7.25	5.0
1300	7.61	9.8	32.9	7.34	5.1
1400	7.69	9.6	33.1	7.42	5.2
1500	7.77	9.9	33.4	7.49	5.3
1600	7.84	9.8	33.6	7.56	5.4

It will be noticed that in the burst size range that we are interested in the effective burst range is essentially a constant and equal to $\eta = 10\ X_0$ whereas the variation of the most probable energy can be approximately represented by $E_{max} = 32\,\beta\,S$. It is interesting to compare these values with those obtained by Christy and Kusaka for μ-bursts. Their analytical approximation (See Ref. 1) to the shower curve gave $\eta = 7X_0$* and $E = 10\,\beta\,S$ which would correspond to a proton energy of $E = 30\,\beta\,S$. This is an illuminating example to show how small is the influence of the special conversion mechanism. Excluding fluctuations the only effect of assuming an

---

* Actually Christy and Kusaka give $\eta = 3.5\ X_0$; but they seem to have dropped a factor of 2 for simplicity as it did not have any influence on their considerations.

initial multiplicity is to increase the effective burst range by 40%.

In the fifth column of Table 4 we have listed for comparison the minimum values of E in the integration for M(S), taken from fig. 3. The last column gives the approximate values of X_1 corresponding to E_{max} obtained by interpolation from fig. 1; we have used these values as the effective $\widetilde{X}_1(S)$'s in Eq. (3.8).

As an application of the effective burst range idea we might justify the approximation (3.3). Since $\eta = 10$ and λ_A is of the order of $\frac{350}{7.5}$ we have $\frac{\Delta x}{\lambda_A} \sim 0.25$ and the error made in replacing $e^{\frac{\Delta x}{\lambda_A}} = 1.28$ by $1 + \frac{\Delta x}{\lambda_A} = 1.25$ is about 2%.

(d) Effect of a second interaction by charged mesons

It is of interest to estimate the contribution to the burst size of the secondary showers initiated by possible collisions of the charged π-mesons present in the narrow cone. For this purpose we may neglect the secondary interactions of the wide cone mesons. Let the collision and absorption mean free paths in lead of charged mesons be ξ; then assuming that after a collision of a charged meson with a lead nucleus one-third of the incoming energy goes into a photon-initiated shower we have for the number of

particles at a distance y from the point of the first collision of a proton of energy E with a lead nucleus,

$$N_{total}(E,y) = \tilde{N}(E,y) + \int_0^y e^{-\frac{x}{\xi}} \frac{dx}{\xi} \; 6N\left(\frac{E}{32}, y-x\right)$$

$$= \tilde{N}(E,y) + \tilde{N}_1(E,y) \qquad (3.10)$$

where $\tilde{N}(E,y)$ is the expected number of particles in all the cascades generated by the first collision and was computed previously, the integral represents the contribution of the secondary interactions due to 6 charged mesons in the narrow cone and $N(\frac{E}{32}, y-x)$ gives the expected number of particles at a thickness y-x in a shower initiated by a photon of energy $\frac{0.85}{3 \times 9} E = \frac{E}{32}$.

To evaluate the integral, we have used the approximate formula for $N(E,u)$ given by Christy and Kusaka which is good for $E = 10^{10} - 10^{11}$ ev:

$$N(E,u) = \left\{ 1 - \left(1 - \frac{9\beta}{E}\right) \left(\frac{u}{7}\right)^{\frac{58\beta}{E}} e^{\frac{58\beta}{E}\left(1-\frac{u}{7}\right)} \right\}^{-1} \qquad (3.11)$$

After the substitution y - x = u we obtain for $\tilde{N}_1$

$$\tilde{N}_1(E,y) = \frac{6}{\xi} e^{-\frac{y}{\xi}} \int_0^y \frac{e^{\frac{u}{\xi}} du}{1 - c\left(\frac{u}{7} e^{-\frac{u}{7}}\right)^b} \qquad (3.12)$$

where

$$a = 1 - \frac{9 \times 32\beta}{E}$$

$$b = \frac{58 \times 32\beta}{E}$$

$$c = a\, e^b$$

The integral can now be easily carried out numerically. Table 5 lists the results for $\xi = 27.2$ sh.u. $\sim$ 200 gm/cm^2 and an initial energy of $\frac{E}{32} = 1198\ \beta$ corresponding to $\varepsilon = 7.5$; the values of $\tilde{N}(\varepsilon, y)$ are also given for comparison. The value of 200 gm/cm^2 for the mean free path of Λ-mesons is consistent with cloud-chamber observations on the nuclear interactions of the penetrating secondaries produced by cosmic rays. (Ref. 29)

Table 5

y	$\tilde{N}_1(y)$ for $\varepsilon = 7.5$	$\tilde{N}(y)$ for $\varepsilon = 7.5$
3	13	510
4	26	880
5	44	1210
6	66	1440
7	92	1510
8	117	1460
10	155	1110
12	177	685
14	187	370
18	188	
22	177	

We have plotted in fig. 1 the corrected cascade curve for $\varepsilon = 7.5$. Noticing that $\varepsilon = 7.5$ gives $\Delta X = 9.20$ for S = 600 which is quite close to the effective burst range we obtain for the correction on ΔX due to secondary interactions:

$$\frac{\Delta X_{cor}}{\Delta X} = \frac{10.45}{9.20} = 1.14 \qquad (3.13)$$

Thus neglecting any possible change with S, one may multiply all frequencies by 1.14 to take care of the contribution of the secondary showers. Any small change in the assumed value of the mean free path for charged mesons would presumably lead to a second order correction in this factor.

(e) Effective path length in the shield

The expression (3.8) for the size-frequency distribution under a thick shield contains in the exponential absorption factor a, the thickness of the shield. The question arises as to the thickness that must be used for a spherical shield since it is not the same for all rays in a given direction. Neglecting the scattering one can obtain an effective path length as follows:

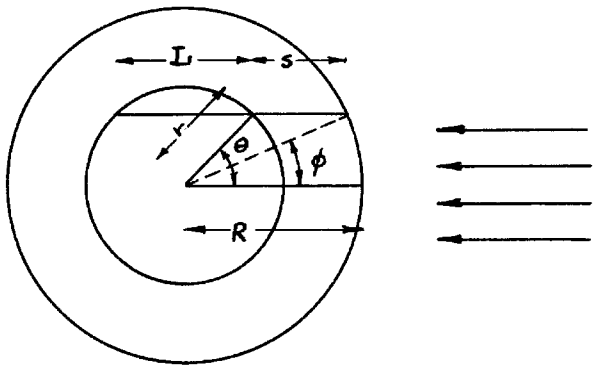

Let r be the radius of the ionization chamber, R - r the thickness of the shield, s the path length in the shield for a primary particle coming in the indicated direction, L its path length in the chamber and θ, ϕ the polar angles

as indicated in the figure, the polar axis being drawn along the radius in the direction of the incoming particles. The number of particles with a path length of s will first be proportional to the area of the ring given by $\theta, d\theta$, i.e. to

$$2\pi r \sin\theta \cdot r\, d\theta \cos\theta = 2\pi r^2 \sin\theta \cos\theta\, d\theta$$

Secondly* the influence of these particles on the observed ionization will depend on L. The ionization is proportional to LS or consequently to LE where E is the energy of the incoming particle. As we are interested in bursts of size greater than a definite S we are recording only ionizations larger than a definite $I = \propto lE$, $\propto$ being a proportionality factor. Hence a shower that goes through L in the chamber must have at least an energy of $E = I/\propto L \sim 1/L$ to produce an observable burst and the number of particles capable of generating such showers is proportional to $1/E^2$, or consequently to L^2. We thus obtain a weighting factor of L^2. The effective path length in the shield is then given by

$$\bar{s} = \frac{\int_0^{\frac{\pi}{2}} 2\pi r^2 \sin\theta\cos\theta\; s\, L^2\, d\theta}{\int_0^{\frac{\pi}{2}} 2\pi r^2 \sin\theta\cos\theta\; L^2\, d\theta} \qquad (3.14)$$

---

* I am indebted to Professor Christy for reminding me of this point.

which upon inserting

$$s = \sqrt{R^2 - r^2 \sin^2\theta} - r\cos\theta$$
$$L = 2r\cos\theta \qquad (3.15)$$

and integrating becomes

$$\bar{s} = \frac{4}{15r^4}\left\{2(R^2-r^2)^{5/2} - R^3(2R^2-5r^2)\right\} - \frac{4r}{5} \qquad (3.16)$$

In the third column of the following Table 6 we give the effective path lengths as computed by (3.16), corresponding to the various chambers and shields that we shall be dealing with in Parts II and III.

Table 6

r (cm)	R-r (cm)	$\bar{s}$ (cm)	$\bar{s}_1$ (cm)
7.62	11.74	12.59	12.94
17.5	11.95	13.63	14.37
17.5	27.95	29.74	31.11

The fourth column lists effective path lengths computed by using a weighting factor of L which corresponds to an integral primary spectrum of 1/E.

Part II. Air bursts

4. Introduction

Coincidence experiments with shielded spherical ionization chambers surrounded by counters by Lapp (Ref. 4) and Fahy and Schein (Ref. 30) showed that apparently both at sea level and at 3500 meters less than 5% of the bursts with more than 200 particles were coincident with air showers. Similarly at 30,000 feet McMahon, Rossi and Burditt (Ref. 31) in experiments with a cylindrical chamber placed under a hemispherical shield and a coincidence counter arrangement found that a negligible fraction of the bursts with more than 60 particles coincided with air showers. However, as one could not be sure that the counter system used to detect the air showers in these experiments was fully effective, there remained some doubt as to the actual contribution of air showers to the observed bursts. Also Fahy and Schein (Ref. 32) obtained at 3500 m. 4 bursts with more than 4000 particles out of which 3 were coincident with giant air showers. This indicated an increase in the relative importance of air showers with the burst size, which fact, if true, could help to explain the very low coincidence ratio observed by Rossi et al. For these reasons it seemed worth while to try to compute a theoretical size-frequency

distribution for air bursts at 30,000 feet. While this work was in progress, Fahy (Ref. 33) and later Stinchcomb (Ref. 58) by means of a more effective coincidence arrangement and several absorbers of various thicknesses obtained the variation with burst size of the percentage of the bursts accompanied by air showers. Their work establishes two points: (1) The percentage of bursts accompanied by air showers increases with burst size. (2) The majority of such bursts are generated by the penetrating component of air showers. As we have been implicitly assuming that the coincident bursts are mostly due to the soft component, this second conclusion reduces the relative importance of our calculations on air bursts in analyzing burst data. We shall show however that it is not incompatible with them.

5. Analytical formulation of the size-frequency distribution.

We shall follow a procedure first developed by Cocconi (Ref. 39) in interpreting the density spectrum of extensive showers as obtained by counters and later applied to the case of lightly shielded ionization chambers by Amaldi and his collaborators (Ref. 35). This approach is based on the observation that since the density of particles in an extensive shower decreases as one moves away

from the shower axis, if a specific shower has enough density to produce an effect of a given size S at a radial distance r from the axis, it will produce an effect of size larger than S at all points within a circle of radius r. Therefore an integral size-frequency distribution can be obtained simply by evaluating integrals of the type

$$\int_{E_s}^{\infty} P(\epsilon)\, d\epsilon \quad \pi r^2(\epsilon, t) \tag{4.1}$$

where $P(E)dE$ gives the number of primary particles with energies between E and E + dE which initiate the showers at a point t shower units above the observation point. In our case these showers must contain more than S particles after crossing the thick shield surrounding the spherical ionization chamber so as to produce bursts of size greater than S.

By attempting to apply our multiple production model to the initiation of extensive showers we introduce a complication into the previous simple picture. However the possible constructive interference effects between the showers initiated by different photons, which would make it very hard to determine r(E,t), can be largely neglected in our case, due to the following considerations. On the one hand, the large thickness of the lead shield eliminates the effect of the low energy particles and photons in the extensive shower; so that to produce the required

multiplication in going through the shield a shower must effectively hit the chamber with its core. On the other hand, by the time they arrive at the altitude of the chamber the different cores will most likely be separated from each other by distances large compared to the chamber diameter. From the Schein star (Ref. 11) we obtain an initial angular divergence of 0.001 rad. between two photons of energy $\sim 10^{12}$ ev. The air bursts are predominantly due to photons of initial energies $\sim 10^{11}$ ev. Now according to all the theories on multiple production the initial divergence would be a decreasing function of of the energy; if we assume an inverse proportionality (as suggested by Professor Christy) we deduce an angle of 0.01 rad. for our energies. Such an initial divergence between two photons would result after going through a distance of one shower unit (which is $\sim$ 900 m. at 30,000 feet, $\sim$ 500 m. at 3500 m. and 330 m. at sea level) in a separation between two shower cores of $\sim$ 1800 cm at 30,000 feet, 1000 cm at 3500 m. and 660 cm at sea level; these separations are much larger than the diameters of the two chambers used in burst experiments which are 15 cm for the Neher chamber and 35 cm for the Carnegie Model C meter. Therefore as a first approximation at least, we can ascribe each burst to one and only one photon-initiated shower. Such an

approximation might result in too low a burst rate especially for large chambers at low altitudes.

Consider now bursts of size larger than S due to showers initiated by decay photons produced in collisions $t_{sh.u.}$ above the chamber. In view of their low energies the photons of the wide cone (See Part I,1) can be neglected here; also for simplicity 1/3 of the incoming energy will be assumed to go into the 6 photons of the narrow core, each getting an energy of E/18. We may reasonably assume that the cores of the showers initiated by these photons will be uniformly spread over a circle of radius R when they reach the altitude of the chamber. Let r be the radius corresponding to the burst size S for a shower of energy E/18 and distance t (which, as indicated above, differs very little from the actual chamber radius); we draw a circle of radius R - r around the center of the cross section of the ionization chamber. Then, as is clearly seen from the accompanying figure, for any primary

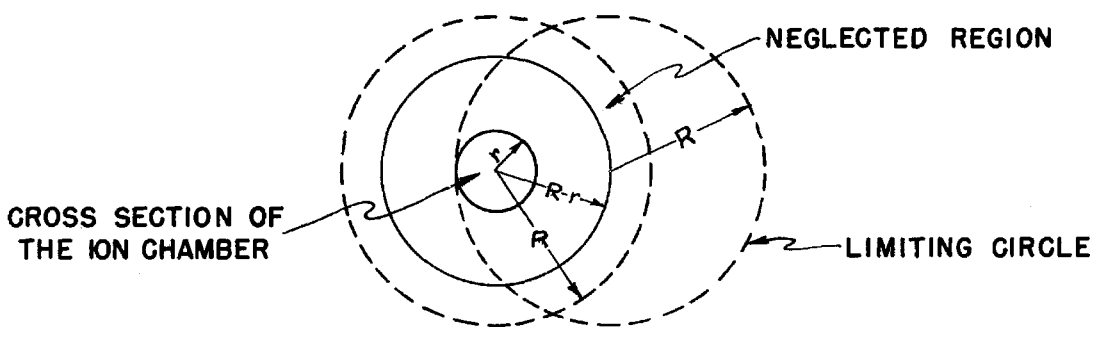

collision taking place at any point inside this circle, t sh.u. above the chamber, the probability of producing a burst of size larger than S will be proportional to

$$\frac{6\pi r_s^2(E,t)}{\pi R^2(t)} \qquad (4.2)$$

Consequently the number of bursts of size larger than S, due to collisions t sh.u. above the chamber, will be proportional to

$$\int_{E_s}^{\infty} \frac{6\pi r_s^2(E/18,t)}{\pi R^2(t)} \pi (R-r)^2 P(E)\,dE \qquad (4.3)$$

where $P(E)dE$ is the differential spectrum of primary protons t sh.u. above the chamber; or since $R \gg r$ (4.3) approximately reduces to

$$\int_{E_s}^{\infty} 6\pi r_s^2\left(\frac{E}{18},t\right) P(E)\,dE \qquad (4.4)$$

As this result is independent of R(t) we are back to the case of no initial multiplicity and all it remains to do is an integration over t and over the zenith angles.

Let t_A be the absorption mean free path in air of the primary radiation as before and t_c its collision mean free path in air. Then using the accompanying figure, it may easily be seen that $H(>S)$, the frequency of the air bursts of size greater than S is given by

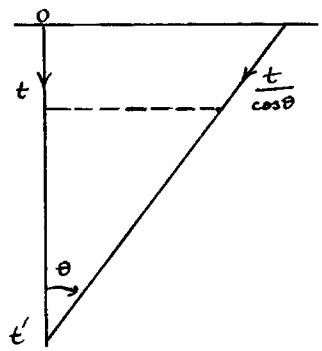

$$H(>S) = \int_0^{\frac{\pi}{2}} 2\pi \sin\theta \, d\theta \int_0^{t'} e^{-\frac{t \sec\theta}{t_A}} \frac{dt \sec\theta}{t_c} \int_{E_S}^{\infty} 6\pi r_S^2 \left[\frac{E}{18}, (t'-t)\sec\theta\right] \frac{P_0}{E^3} dE \quad \text{per sec.}$$

(4.5)

where t is the vertical distance in sh.u. measured from the top of the atmosphere, t' the altitude of the ionization chamber measured in the same way, θ the zenith angle of the direction of the incoming beam and $r_S\left[\frac{E}{18},(t'-t)\sec\theta\right]$ is evaluated specifically for the chamber whose burst frequency is expressed by H(> S). We carry out calculations with only $\frac{P_0}{E^3} dE$ as this type of spectrum seems to be best suited to explain the shield bursts (Sec. 3.b). Making the substitutions

$$(t'-t)\sec\theta = T \quad , \quad -dt \sec\theta = dT$$

and

$$\frac{E}{18} = \beta e^{\varepsilon}$$

one finds

$$H(>S) = \frac{\pi^2 P_0}{27 \beta^2 t_c} \int_0^{\frac{\pi}{2}} \sin\theta \, d\theta \int_0^{t' \sec\theta} e^{-\frac{t' \sec\theta - T}{t_A}} dT \int_{\varepsilon_s}^{\infty} r_s^2(\varepsilon, T) \, e^{-2\varepsilon} d\varepsilon \quad \text{per sec.} \tag{4.6}$$

where T is now the distance over which the showers develop and β is the critical energy in lead. Defining for ease in calculations the functions $f_S(T)$ and $g_S(\theta, t')$ as

$$f_s(T) = \int_{\varepsilon_s}^{\infty} r_s^2(\varepsilon, T) \; e^{2(13-\varepsilon)} \, d\varepsilon \tag{4.7}$$

and

$$g_s(\theta, t') = \int_0^{t' \sec\theta} e^{-\frac{t' \sec\theta - T}{t_A}} f_s(T) \, dT \tag{4.8}$$

one obtains finally

$$H(>S) = \frac{\pi^2 e^{-26}}{27} \frac{P_0}{t_c \beta^2} \int_0^{\frac{\pi}{2}} g_s(\theta, t') \sin\theta \, d\theta \quad \text{per sec.} \tag{4.9}$$

6. Evaluation of $f_S(T)$

This is the main part of the calculations as it involves the lateral structure of the extensive showers and we shall present it in some detail. One unfortunate aspect of the computation might be mentioned here: As it turns out, $f_S(T)$ depends very sensitively on the shield thickness

so that strictly speaking the whole computation is valid for only one thickness; thus its usefulness is severely limited, especially considering the uncertainty in the size of the shower unit in lead which makes the shield thickness somewhat uncertain. We shall try, in the end, to remedy this defect with an approximate method of extending the result to other thicknesses.

(a) Lateral distribution. We begin by a discussion of the lateral spread of extensive showers. Let $p(E,r)$ be the radial distribution function for particles (or photons) with the same energy E, i.e. the probability that a particle (or photon) of energy E be found in a unit square at a radial distance r from the shower axis. r is measured in lateral shower units for which we find from a table given by M. Mills* (Ref. 37) $x = 178$ m at 33,000 ft and use this value at 30,000 feet to take care of the density variation in the atmosphere. $p(E,r)$ must be normalized to give $\int p(E,r)\, 2\pi r\, dr = 1$. The density of particles (or photons) with energies between E and $E + dE$ may now be obtained as

---

* Strictly speaking, Mills' figures must be decreased in the ratio 37.3/43 to correct for the contribution of atomic electrons in the bremsstrahlung and pair creation processes; however such a change would not have any effect in the value of $f_S(T)$, as will be seen presently.

$$\rho(E,r)\,dE = \pi(W_0, E, T)\; p(E,r)\,dE \qquad (6.1)$$

where $\pi(W_0,E,T)dE$ is the average number of particles (or photons) with energies between E and E + dE at thickness T in a shower initiated by a photon of energy W_0.

For p(E,r), a Gaussian of the form

$$p(E,r) = \frac{1}{\pi \overline{r^2}(E)}\; e^{-\frac{r^2}{\overline{r^2}(E)}} \qquad (6.2)$$

will be used, where the mean square radial spread $\overline{r^2}(\epsilon) = a^2 \frac{E_s^2}{E^2}$ with E_s = 21 Mev and $a_{el}^2 = 0.642$, $a_{ph}^2 = 1.13$ for electrons and photons respectively, is taken from the calculations of Nordheim and Roberg (Ref. 17) who obtained it directly by means of a self-comsistent method of treating the electron scattering. It is known that the actual distribution function differs widely from a Gaussian over the whole radial extension of the shower, mainly owing to the occasional large single scatterings and to the influence of earlier generations (See e.g. Moliere's article in Heisenberg's book,Ref. 38). However in the immediate vicinity of the shower axis where multiple scattering predominates over single scattering a Gaussian may be expected to be a good approximation. In fact as Moliere points out, the radial density function for all shower

particles that one obtains from a Gaussian distribution for p(E,r) has the same singularity of 1/r near the axis as his more accurate density function. Since our purposes require a lateral extension only up to $r \sim 10^{-3}$ we feel justified in using a Gaussian distribution.

$f_S(T)$ can be determined by good approximate methods for either $T \leq 2$ or $T \geq 6$. The remaining part can be obtained by graphical interpolation. In this section we shall use the shower formulae given by Rossi and Greisen (Ref. 36) (R - G in short) whose expression for the total number of particles is nearly identical with that of Snyder and who in addition give the energy distribution of the shower particles and photons. We are going to determine $f_S(T)$ for $S = 400$ and $S = 700$ for the Neher chamber which has a radius of r = 7.62 cm and which will be assumed to be surrounded by a lead shield 22.7 sh.u. thick.

(b) Computations for $T \leq 2$.

When the shower does not have time to develop appreciably in the air before reaching the shield of the ionization chamber we may neglect both its lateral extension and its transition effect in passing from air into lead. Thus the actual radius r_o may be taken as $r_S(\varepsilon)$ for all sizes and energies with ε_s determined from the simple longitudinal development formula as the minimum energy that would produce

S particles after going through 22.7 + T sh.u. of lead. This calculation is certainly correct for T = 0 and we shall somewhat arbitrarily take it as approximately valid up to T = 2 after which mainly the lateral spread of the shower in the air will make $f_s(T)$ deviate toward lower values.

We have therefore from (4.7)

$$f_s(T) = r_0^2 \int_{\varepsilon_s}^{\infty} e^{2(\beta-\varepsilon)}\, d\varepsilon = \frac{r_0^2}{2} e^{2(\beta-\varepsilon_s)} \qquad (6.3)$$

Using R - G formulae for the number of particles at thickness u we obtain the following Table 7 for the required minimum energies and the resulting values of $f_S(T)$.

Table 7

T	u	ε_{400}	ε_{700}	f400(T)	$f'_{400}(T)$
0	22.7	10.93	11.33	576 x 10^{-8}	259 x 10^{-8}
1	23.7	11.14	11.53	378	174
2	24.7	11.44	11.77	208	107

(c) Computations for $T \geq 6$

This is the region in which the air shower has sufficiently developed so that the major contribution to a burst under the lead shield comes from medium energy particles and photons of the air shower whose differential spectrum can be well represented by the R - G expressions.

Our procedure consists in determining S(r), the number of particles that penetrate into the chamber as a function of r for several initial energies (ε) and in inverting these plots graphically to obtain $r_S(\varepsilon)$ for S = 400 and S = 700.

For an air shower whose axis is at a distance r from the center of the ionization chamber, the density of the particles penetrating to the chamber will be clearly given by

$$\rho(r) = \int_{E_e}^{W_o} \frac{E^2}{\pi a_{el}^2 E_s^2} e^{-\frac{r^2 E^2}{a_{el}^2 E_s^2}} \pi(W_o, E, T)\, dE\ \Pi(E, o, T') + \int_{W_e}^{W_o} \frac{W^2}{\pi a_{ph}^2 E_s^2} e^{-\frac{r^2 W^2}{a_{ph}^2 E_s^2}} \pi(W_o, W, T)\, dW\ \Pi(W, o, T') \tag{6.4}$$

where we are using the well-known notation of R - G for the differential and integral spectra in which E refer to particle energy and W to photon energy; T is the thickness in air, T' the thickness in lead (22.7 sh.u.) and E_e, W_e are convenient lower energy limits for the shower particles and photons. As the sharply peaked distribution of the Gaussian dominates over the slowly varying product of spectra, the integrals are effectively evaluated around the maxima of the Gaussians, i.e. around the values

of E and W that give $\frac{r^2E^2}{a_{el}^2 E_s^2} = 1$ and $\frac{r^2W^2}{a_{pl}^2 E_s^2} = 1$ respectively which are found to be

$$E_c = \frac{1.7\times10^7}{r}\ ev \quad , \quad W_c = \frac{2.2\times10^7}{r}\ ev$$

Corresponding to $r = 10^{-4} - 10^{-2}$ we obtain $E_c \sim W_c \sim 2 \times 10^9 - 2 \times 10^{11}$ ev. Thus taking the critical energy in air as $\beta_{air} = 100$ Mev, we see that for initial energies ranging from $W_o = 2 \times 10^{12}$ upwards, the major contribution to the integrals will come from medium energies safely distant from the two extremes of initial and critical energies. We can therefore use R - G expressions for the spectra without any corrections. Also in the differential spectra ionization loss in air can be neglected and the lower limits E_e, W_e may be taken equal to β_{air}. Substituting the R - G spectra we obtain for the part of ρ due to the electrons of the air shower,

$$\rho_{el} = \int_{\beta_{Air}}^{W_o} \frac{E^2}{\pi a_{el}^2 E_s^2}\, e^{-\frac{r^2E^2}{a_{el}^2E_s^2}}\, A_E(s,s')\left(\frac{W_o}{E}\right)^s \frac{dE}{E}\left(\frac{E}{\beta}\right)^{s'} e^{\lambda_1(s)T + \lambda_1(s')T'} \qquad (6.5)$$

where

$$A_E(s,s') = \frac{1}{2\pi}\frac{\sqrt{s}}{s'}\frac{M(s)\,H_1(s')\,K_1(s',-s')}{\left[\lambda_1''(s)\,T - \frac{1}{2s^2}\right]^{1/2}\left[\lambda_1''(s')\,T' + \frac{1}{s'^2}\right]^{1/2}} \qquad (6.6)$$

$$T = -\frac{1}{\lambda_1'(s)}\left(\ln\frac{W_o}{E} + \frac{1}{2s}\right) \qquad (6.7)$$

$$T' = -\frac{1}{\lambda_1'(s')}\left(\ln\frac{E}{\beta} - \frac{1}{s'}\right) \tag{6.8}$$

and $M(S)$, $H_1(S)$, $K_1(S,-S)$, $\lambda_1(S)$, $\lambda_1'(S)$, $\lambda_1''(S)$ are functions tabulated or plotted in the R - G review. To carry out the integration numerically it is convenient to make the substitution

$$\varepsilon = \ln\frac{W_o}{E} \tag{6.9}$$

which gives

$$\rho_{el} = \int_0^{\varepsilon_o} \frac{1}{\pi r^2} A_\varepsilon(s,s') \exp\left\{2(\varepsilon_c-\varepsilon) - e^{2(\varepsilon_c-\varepsilon)} + \varepsilon s + \varepsilon' s' + \lambda_1(s)T + \lambda_1(s')T'\right\} d\varepsilon \tag{6.10}$$

with

$$\varepsilon_o = \ln\frac{W_o}{\beta_{Air}} \tag{6.11}$$

$$\varepsilon_c = \ln\frac{W_o}{E_c} = \ln\frac{r W_o}{a_{el} E_s} \tag{6.12}$$

$$\varepsilon' = \ln\frac{W_o}{\beta} - \varepsilon = \ln\frac{E}{\beta} \tag{6.13}$$

and

$$T = -\frac{1}{\lambda_1'(s)}\left(\varepsilon + \frac{1}{2s}\right) \tag{6.14}$$

$$T' = -\frac{1}{\lambda_1'(s')}\left(\varepsilon' - \frac{1}{s'}\right) \tag{6.15}$$

We have plotted the last two relations for T = 6.8 and T = 9.3 with T' = 22.7 and β = 10 Mev, β_{air} = 100 Mev to obtain the functions S = f(ε), S' = f'(ε'). As $A_\varepsilon(S,S')$ varies slowly, it was taken out of the integration; after the integration was carried out by means of Simpson's rule with intervals of $\Delta\varepsilon = 0.5$, the result was multiplied by $A_\varepsilon(S,S')$ in which the values of S,S' that make the exponential integrand maximum were substituted. A similar procedure gives ρ_{ph} , i.e. the part of ρ due to the photons of the air shower, which must be independently calculated because of the different values of $\overline{r^2}$, $A_\varepsilon(S,S')$ and $\varepsilon = f(S)$, $\varepsilon' = f'(S')$ for photons. The results are listed below in Table 8, in particles per lateral sh.u. square, for T = 6.8, T = 9.3 and for several energies W_o ; they are also plotted in figs. 5 and 6.

Table 8

	r(in l.sh.u.)	$\rho_{el}(r)$	$\rho_{ph}(r)$	$\rho_{total}(r)$
T = 6.8 $W_o = 10^{14}$ ev	3×10^{-4}	8.8×10^8	24.6×10^8	3.34×10^9
	5	1.9×10^8	5.6×10^8	7.5×10^8
	10	2.1×10^7	7.1×10^7	9.2×10^7
T = 6.8 $W_o = 10^{13}$ ev	3×10^{-4}	9.9×10^7	2.8×10^8	3.8×10^8
	5	2.4×10^7	7.2×10^7	9.6×10^7
	10	3.3×10^6	1.1×10^7	1.4×10^7

Table 8 (continued)

	r (in l.sh.u.)	$\rho_{el}(r)$	$\rho_{ph}(r)$	$\rho_{total}(r)$
$T = 9.3$ $W_o = 1.2 \times 10^{14}$	3×10^{-4}	7.0×10^{8}	1.55×10^{9}	2.25×10^{9}
	5	1.8×10^{8}	4.0×10^{8}	5.8×10^{8}
	10	2.3×10^{7}	5.1×10^{7}	7.4×10^{7}
$T = 9.3$ $W_o = 10^{13}$ ev	3×10^{-4}	0.59×10^{8}	1.7×10^{8}	2.3×10^{8}
	5	1.6×10^{7}	5.0×10^{7}	6.6×10^{7}
	10	0.35×10^{7}	0.86×10^{7}	1.2×10^{7}

In the actual computations many approximate short cuts were used, especially in deducing the values for ρ_{ph}, so that the above figures may have errors in them up to 10%, which is a sufficient approximation for our purposes.

It is apparent that the density varies considerably in the region $r = 0 - 10^{-3}$. The assumption of a constant density over the extension of the chamber for deriving from ρ the number of particles S that penetrate into the chamber would thus lead to quite inaccurate results for showers whose axes hit the chamber. In order to account for this effect of the finite size of the chamber we must discuss the case of a shower whose axis passes through the center of the ionization chamber. For such a shower S_{el} and S_{ph} can clearly be obtained by a direct integration over r:

$$S_{e1}(o) = \int_{o}^{r_o} 2\pi r\, dr \int_{\beta_{Air}}^{W_o} \frac{E^2}{\pi a_{e1}^2 E_s^2}\, e^{-\frac{r^2E^2}{a_{e1}^2E_s^2}}\, \pi(W_o, E, T)\, dE\, \Pi(E, o, T') \tag{6.16}$$

$$S_{ph}(o) = \int_{o}^{r_o} 2\pi r\, dr \int_{\beta_{Air}}^{W_o} \frac{W^2}{\pi a_{ph}^2 E_s^2}\, e^{-\frac{r^2W^2}{a_{ph}^2E_s^2}}\, \pi(W_o, W, T)\, dW\, \Pi(W, o, T') \tag{6.17}$$

and $$S(o) = S_{e1}(o) + S_{ph}(o) \tag{6.18}$$

where r_o is the radius of the Neher ionization chamber in lateral units, i.e. $r_o = 4.28 \times 10^{-4}$. Integrating with respect to r one obtains for $S_{e1}(o)$,

$$S_{e1}(o) = \int_{\beta_{Air}}^{W_o} \left(1 - e^{-\frac{r_o^2E^2}{a_{e1}^2E_s^2}}\right) \pi(W_o, E, T)\, \Pi(E, o, T')\, dE \tag{6.19}$$

The spreading influence of the Gaussian is canceled in the integration over r and now the integral is evaluated around the maximum of the product of spectra; this maximum energy though higher than the E_e of the previous calculation is still lower than W_o by about a factor of 10. Inserting therefore the R - G spectra and making the aforementioned substitution we obtain

$$S_{e1}(o) = \int_{o}^{\varepsilon_o} q(r_o, \varepsilon)\, A_\varepsilon(s, s')\, exp\left\{\varepsilon s + \varepsilon' s' + \lambda_1(s)T + \lambda_1(s')T'\right\} d\varepsilon \tag{6.20}$$

where

$$q(r_o, \varepsilon) = 1 - exp\left\{-e^{2\left(\ln \frac{r_o W_o}{a_{e1}E_s} - \varepsilon\right)}\right\} \tag{6.21}$$

and S,S' are given in (6.14) and (6.15). There is a similar expression for $S_{p\lambda}(o)$. The results are shown in Table 7 for T = 6.8, T = 9.3 and several initial energies. One thing that comes out of these calculations is the smallness of the effect of $q(r_o,\varepsilon)$ (which is the factor bringing in the size of the chamber) in determining S. It is found that most of the contribution to the integral (6.16) comes from distances up to $r = 1.5 \times 10^{-4}$. This fact suggests a simple way of obtaining S for a shower whose axis passes through the chamber at a distance r from the center. The accompanying figure shows that for such a shower, S will be given to a good approximation by

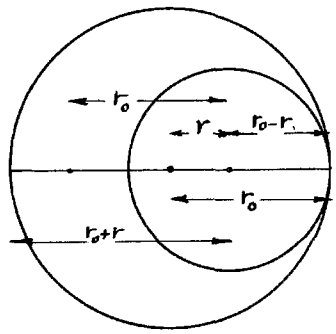

$$S(r) = S_{r_o-r}(o) + \pi\left[r_o^2 - (r_o-r)^2\right]p(r_o) \qquad \text{for} \quad r \lesssim 3\times10^{-4} \tag{6.22}$$

where $S_{r_o-r}(o)$ is given by the integrals (6.16), (6.17) in which r_o is replaced by r_o-r.

As the variation of the density slows down when one

moves away from the axis, it may be considered to be constant over the extension of the chamber for distances larger than the diameter of the chamber, or perhaps for $r \geqslant 10^{-3}$. Thus for $r \geqslant 10^{-3}$ we have simply

$$S(r) = \pi r_0^2 \rho(r) = 5.75 \times 10^{-7} \rho(r) \qquad (6.23)$$

To check this last assumption we have computed S (7.28) for $W_0 = 10^{13}$ev and for T = 6.8, T = 9.3 by the following more accurate method.

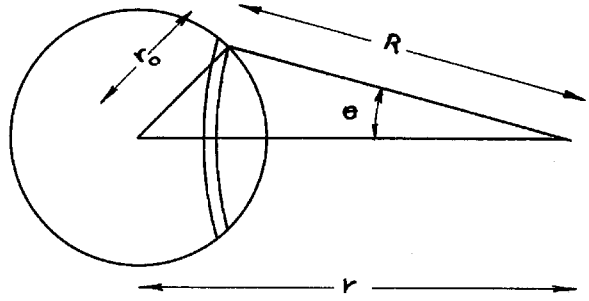

From the figure we have,

$$S(r) = \int_{r-r_0}^{r+r_0} 2R\theta \, dR \, \rho(R) \qquad \text{for} \quad r \geq r_0$$

and using $r_0^2 = R^2 + r^2 - 2Rr \cos\theta$, we find

$$S(r) = 2\int_{r-r_0}^{r+r_0} \rho(R) R \cos^{-1}\left(\frac{R^2+r^2-r_0^2}{2Rr}\right) dR \qquad (6.24)$$

A numerical integration for the cases mentioned gave results in good agreement with the previous more approximate calculations.

The results obtained by means of (6.3), (6.10), (6.20), (6.22), (6.23) and (6.24) are listed in Table 9.

Table 9

	r	$S_{el}(r)$	$S_{ph}(r)$	$S_{total}(r)$
$T = 6.8$ $W_o = 10^{14}$	0	19500	52400	71900
	10×10^{-4}	12	41	53
$T = 6.8$ $W_o = 10^{13}$	0	560	1500	2060
	1×10^{-4}	556	1470	2026
	2	531	1390	1921
	3	479	1230	1709
	7.28			212
	10	1.9	6.4	8.3
$T = 6.8$ $W_o = 6 \times 10^{12}$	0	228	668	896
	1 10			886
	2			805
	3			675
$T = 6.8$ $W_o = 3.64 \times 10^{12}$	0	102	300	402
	1×10^{-4}	94	284	378
$T = 9.3$ $W_o = 1.2 \times 10^{14}$	0	11400	25400	36800
	1×10^{-4}			36400
	2			35200
	3			32600
	728			155
	10	14	29	43
$T = 9.3$ $W_o = 10^{13}$	0	214	495	709
	1×10^{-4}			690
	2			639
	3			546
	7.28			19
	10	2.0	4.9	6.9

Table 9 (continued)

	r	$S_{el}(r)$	$S_{ph}(r)$	$S_{total}(r)$
$T = 9.3$ $W_0 = 7 \times 10^{12}$	0			400
$T = 9.3$ $W_0 = 6 \times 10^{12}$	0	73	197	270
	1×10^{-4}			257
	2			242
	3			196

The remark about the errors in Table 8 applies also to Table 9. In figures 5 and 6, the variation of S(r) with r for several energies is shown as obtained from Table 7 and plotted in terms of an effective density defined so as to coincide with the actual density for large r, namely as $\rho_{eff}(r) = \frac{1}{\pi r_0^2} S(r) = \frac{10^7}{5.75} S(r)$. Curves in dashed line represent the actual density as obtained from Table 6. By means of these plots it is easy to derive the variation of $W_0(r)$ with r for S = 260, S = 400 and S = 700 as shown in the figures 7 and 8 for T = 6.8 and T = 9.3. The appearance of these curves substantiates our initial assumption as to the core-selecting property of the thick shield; thus in the region $r = 0 - 3 \times 10^{-4}$ where the shower core is hitting the chamber essentially the same minimum energy is needed to produce the given size burst, but after

$r \approx 3 \times 10^{-4}$ the necessary energy rises sharply and for a shower whose axis is away from the center by one diameter it has already increased by a factor of 100.

Finally using the plots in figs. 7 and 8 a numerical integration yields $f_S(T)$ for $S = 400$, $S = 700$ and $T = 6.8$, $T = 9.3$. The details of this integration may be seen in fig. 9 where we have plotted the integrand of $f_S(T)$ (multiplied by 10^8) for $S = 400$, $S = 700$ and $T = 6.8$, $T = 9.3$. The following Table 10 lists all the values of $f_S(T)$ so far obtained.

Table 10

T	$f_{400}(T)$	$f_{700}(T)$
0	576×10^{-8}	259×10^{-8}
1	378	174
2	208	107
6.8	8.80	4.45
9.3	2.59	1.26

These points are plotted in fig. 10 and a smooth curve is drawn through them to obtain the functions $f_{400}(T)$ and $f_{700}(T)$ throughout the region of interest $0 \leq T \leq 10$.

7. Evaluation of $g_S(\theta,t')$

The substitution $\tau = t'\sec\theta$ in (4.8) yields

$$g_s(\tau) = \int_0^\tau e^{-\frac{\tau-T}{t_A}} f_s(T)\, dT \qquad (7.1)$$

To carry out the integration numerically, we have to know the value of t_A. However a useful approximate integration can be done if we try to represent $f_S(T)$ by an exponential of the form

$$f_s(T) = F_s\, e^{-\frac{T}{1.65}} \qquad (7.2)$$

where 1.65 is taken from the plots in fig. 10. Inserting this in (7.1) one obtains

$$g_s(\tau) = F_s\, e^{-\frac{\tau}{t_A}} \int_0^\tau e^{-\frac{T}{\alpha}}\, dT \qquad (7.3)$$

$$\text{where} \qquad \alpha = \frac{1.65\, t_A}{t_A - 1.65} \qquad (7.4)$$

and integrating,

$$g_s(\tau) = \alpha F_s\, e^{-\frac{\tau}{t_A}} \left(1 - e^{-\frac{\tau}{\alpha}}\right) \qquad (7.5)$$

which for $\tau \gg \alpha$ reduces to

$$g_s(\tau) \cong \alpha F_s\, e^{-\frac{\tau}{t_A}} \qquad (7.6)$$

$\tau \gg \alpha$ would be satisfied if $t' \gg \alpha$ is satisfied. But as t_A is expected to be $\sim$ 3.5 - 4.5 (corresponding to 130 - 170 gm/cm^2) α might be $\sim$ 2.6 - 3.1 and the condition $t' \gg 3$ is indeed satisfied in the whole region of interest, i.e. from sea level ($t' = 27.7$) up to 30,000 feet ($t' = 8.2$). At 30,000 feet the neglected factor $1 - e^{-8.2/3}$ amounts to $\sim$ 0.06.

From (4.9) and (7.6) we obtain for the size-frequency distribution of air bursts,

$$H(>S) = \frac{\pi^2 e^{-26}}{27} \frac{P_0 \alpha F_S}{t_e \beta^2} \int_0^{\frac{\pi}{2}} e^{-\frac{t' \sec\theta}{t_A}} \sin\theta \, d\theta \qquad (7.7)$$

$$= \frac{\pi^2 e^{-26}}{27} \frac{\alpha F_S P_0}{t_e \beta^2} \mathcal{J}(t'/t_A) \quad \text{per sec.} \qquad (7.8)$$

which brings out the interesting result that the altitude variation of air bursts is the same as that of shield bursts from sea level up to 30,000 feet. Thus the ratio of air bursts to shield bursts should be independent of altitude for the Neher chamber. It is true that because of the altitude variation in the size of the lateral shower unit and the consequent decrease in the lateral extension of air showers for lower altitudes, $f_S(6.8)$ and $f_S(9.3)$ are different at lower altitudes from what we

calculated at 30,000 feet. However as $g_S(\tau)$ is mainly determined by values of $f_S(T)$ for $T \leq 2$, the influence of this change on $g_s(\tau)$ is expected to be negligible in the first approximation.

To estimate the influence of the approximation (7.2) on this result we have integrated (7.1) numerically for $t_A = 4.55$ and for several values of $\tau \geq 8.2$. As may be seen in fig. 11, the results can be well represented by the expression

$$g_{\substack{400\\700}}(\tau) = A_{\substack{400\\700}}\, e^{-\frac{\tau}{4.65}} \qquad \text{for } \tau \geq 8 \qquad (7.9)$$

The slight increase of the exponential length from 4.55 to 4.65 has a negligible effect on $J(t'/t_A)$. Thus, owing to the iterating influence of the integral, $g_s(\tau)$ can be approximated by a simple exponential much better than the original $f_S(T)$ could be. From fig. 11 we also obtain the values of F_{400}, F_{700} by fitting the expression (7.6) to the curves at $\tau = 8.2$; we find

$$\begin{aligned} F_{400} &= 615 \times 10\text{-}8 \\ F_{700} &= 310 \times 10^{-8} \end{aligned} \qquad (7.10)$$

8. Extension to other chambers and shields

So far we have considered only Neher's ionization

chamber with a radius of $r_o = 4.28 \times 10^{-4}$ and a lead shield of thickness $T' = 22.7$. In the evaluation of $f_s(T)$ we made explicit use of T' for $T \leq 2$ and of both r_o and T' for $T \geq 6$. The part for $T \leq 2$ can be easily extended to other thicknesses as it does not involve the lateral extension of the air shower, but the part for $T \geq 6$ can not be extended to other chambers or thicknesses without going through the whole calculation. Again because of the small influence of the actual values of $f_S(T)$ for large T in determining $g_S(\tau)$, a first approximation will be obtained by neglecting the effects of the different lateral distributions. Then two size-frequency distributions belonging to two different arrangements will differ by a constant factor determined by the ratio

$$\frac{f_s^{(1)}(o)}{f_s^{(2)}(o)} = \frac{e^{-2\varepsilon_s^{(1)}}}{e^{-2\varepsilon_s^{(2)}}} = e^{2\Delta\varepsilon_s^{(12)}} \qquad (8.1)$$

where $\Delta\varepsilon_s^{(12)}$ is the difference between the minimum energies for the two shields, provided the frequencies are expressed in bursts per cm^2. Of course this scheme can only be applied when the differences between the two radii and shield thicknesses are not so large as to modify the distinctive character (core-selecting property) of such events. As the two chambers considered in our analysis

satisfy this requirement we shall use it to obtain the ratio of air bursts to shield bursts for the actual shields used with the Neher chamber and with the Carnegie model C meter.

9. Ratio of air bursts to shield bursts for Neher's ion chamber.

From (3.8), (3.13) and (7.8) divided by $\pi r_o^2 = 18.3\,\pi \times 10^{-8}$ we derive for the ratio of air bursts to shield bursts

$$\frac{H(>s)}{N(>s)} = \frac{e^{-26}\times(21.2)^2\times 10^8}{2\times 27\times 18.3\times 1.14}\,\frac{\beta_N^2}{\beta_H^2}\,\frac{F_s}{M(s)}\,\frac{\alpha\lambda_c}{t_c}\,e^{\frac{a}{\lambda_A}}\,e^{-\frac{\tilde{\chi}_1(s)}{\lambda_A}}\,\frac{f_s(a_{Neher})}{f_s(22.7)}$$

$$= 2.47\times 10^{-4}\,\frac{F_s}{M(s)}\,\frac{\alpha\lambda_c}{t_c}\,e^{\frac{a}{\lambda_A}}\,e^{-\frac{\tilde{\kappa}_1(s)}{\lambda_A}}\,\frac{f_s(a_{Neher})}{f_s(22.7)} \qquad (9.1)$$

The Neher chamber was surrounded with 0.31 cm of iron (inner wall), 10.16 cm of lead (shield) and 1.27 cm of iron (outer wall). According to Table 6, the total absorber thickness of 11.74 cm corresponds for this chamber to an effective thickness of 12.59 cm which when subdivided proportionately into its different parts gives from the center outward 0.33 cm of iron, 10.90 cm of lead

and 1.36 cm of iron. The effect of the inner wall is to change β slightly and need not concern us here. The outer wall, as far as shield bursts are concerned, acts simply as an added absorber for the primary radiation since the generation of bursts takes place in the part of the lead shield immediately surrounding the chamber. (See remark at the end of section 3 b). Consequently we have for the Neher chamber

$$e^{-\frac{a}{\lambda_A}} = e^{-\left(\frac{a}{\lambda_A}\right)_{Fe}} \times e^{-\left(\frac{a}{\lambda_A}\right)_{Pb}} = 0.951 \times 0.705 = 0.670 \qquad (9.2)$$

where we have used $\lambda_{Pb} = 350$ gm/cm^2 and $\lambda_{Fe} = 210$ gm/cm^2 (See section 14).

On the other hand for air bursts the outer wall acts as part of the shower producing region, being equal to $\frac{1.36 \times 7.7}{13.9} = 0.75$ sh.u. As the showers going through the outer wall are mostly at the beginning of their development we neglect any transition effects that might occur in entering from air into iron or from iron into lead and simply add the thickness of iron in sh.u. to the thickness of the lead shield in sh.u. We thus obtain a total shield thickness of 18.1 sh.u. Consequently we have for the conversion factor

$$\frac{f_s(a_{Neher})}{f_s(22.7)} = \frac{f_s(18.1)}{f_s(22.7)} = 8.3 \qquad (9.3)$$

In Part III we shall present evidence for adopting the values $\lambda_A = \lambda_c = \frac{350}{7.5}$ sh.u. and $t_A = t_c = \frac{180}{37.3}$ sh.u. Using these values and substituting (9.2), (9.3) in (9.1) we find

$$\frac{H(>s)}{N(>s)} = 0.074 \; e^{-\frac{\tilde{x}_1(s)}{46.7}} \; \frac{F_s}{M(s)} \tag{9.4}$$

and from (7.10) and Table 3 we obtain finally

$$\frac{H(>400)}{N(>400)} = 0.03 \qquad \text{or} \qquad \left(\frac{H}{H+N}\right)_{400} = 0.029$$

$$\frac{H(>700)}{N(>700)} = 0.049 \qquad \text{or} \qquad \left(\frac{H}{H+N}\right)_{700} = 0.047 \tag{9.5}$$

These points are plotted in fig. 13 and joined by a straight line. This plot will be used for correcting the Neher-Biehl data for air bursts from sea level up to 30,000 feet.

10. Comparison with coincidence experiments

Fahy and later Stinchcomb made burst experiments at 3500 m using a heavily shielded Carnegie model C meter together with G-M tube coincidence circuits and determined the percentage of bursts coincident with air showers. The figures obtained for this percentage by the two observers agree with each other within statistical errors; therefore we confine ourselves to the discussion of Stinchcomb's data which have somewhat better statistics. Stinchcomb

obtained the variation with burst size of this percentage when the chamber was shielded by 10.7 cm of lead and also when it was shielded by 130 gm/cm^2 of iron in addition to 10.7 cm of lead. The interesting result was that the addition of 130 gm/cm^2 of iron (9.5 sh.u.) caused only a slight decrease in the coincidence ratio; for instance the percentage changed from 5.2 ∓ 0.8 % to 4.1 ∓ 0.8 % for $S = 400$, from 10 ∓ 2 % to 8 ∓ 3 % for $S = 1000$ and from 56 ∓ 31 % to 50 ∓ 33 for $S = 4000$. As pointed out by Stinchcomb, this fact indicates that the majority of the bursts accompanied by air showers are due to the penetrating component of air showers (presumably composed of high energy nucleons and π-mesons). The extra absorber of 9 sh.u. would cut down the frequency of the bursts due to the soft component of air showers (i.e. air bursts) by a factor of ~ 10 according to (8.1). Therefore only the small difference between the two cases must be due to air bursts; a percentage which increases from 1% for $S = 400$ to 2% for $S = 1000$. Now this is not incompatible with our theoretical estimate. Using an effective shield thickness of 138 gm/cm^2 = 19.4 sh.u. which gives a conversion factor of $\frac{f_S\ (\text{Neher})}{f_S\ (\text{Carnegie})} = \frac{f_S\ (18.1)}{f_S(19.4)} = 1.8$, we deduce from (9.5),

$$\left(\frac{H}{N + H}\right)_{\text{Carnegie}} = 1.6\% \quad \text{for } S = 400$$

and $$\left(\frac{H}{N + H}\right)_{\text{Carnegie}} = 2.6\% \quad \text{for } S = 1000$$

The experimental percentage includes some contributions from μ-bursts and secondary nucleon or pion bursts. But the poorness of the statistics makes it meaningless to try to sort out the pure ratio $\left(\frac{H}{N + H}\right)_{\text{Carnegie}}$ from the experimental percentage. All we can say is that there is agreement between theory and experiment as to the order of magnitude and kind of variation with burst size of the ratio of air bursts to shield bursts.

Part III. Analysis of data

11. Introduction

In this part some unpublished burst data obtained by Neher and Biehl will be presented and analyzed on the basis of ideas developed in the first two parts. For this purpose Christy and Kusaka's calculations for μ-bursts will have to be revised. The absorption mean free path in lead for primary protons in the energy range 10^{11} - 10^{12} ev will be deduced from Fahy's absorption experiments and the absorption mean free path in air will be deduced from the altitude variation of the Neher-Biehl data. Finally, after assuming a value for the primary intensity, the theoretical burst rates will be compared to the burst rates deduced from the Neher-Biehl data.

12. The data of Neher and Biehl

Neher and Biehl obtained the size-frequency distribution of bursts at sea level (1033 gm), at mountain tops (altitude 14,500 feet or 616 gm, which is the average of data at Andes 14,700 feet, 612 gm and Pike's Peak 14,100 feet, 621 gm) and in airplane flights at 30,000 feet, 307 gm. The ionization chamber used in these experiments was a steel sphere of inside radius 7.62 cm and

wall thickness 0.31 cm whose two halves were held together by a steel ring of diameter 2.54 cm. A spherical shield of thickness 10.16 cm made of solid lead and enclosed in a steel shell of wall thickness 1.27 cm surrounded the chamber completely. The chamber was filled with 10 atmospheres of argon in the 307 gm experiments and by 30 atmospheres of air in the others. At one altitude observations were made at places with different latitudes, so that the data are effectively averaged over latitudes.

Owing to the rarity of such events the statistics are not as good as it would be desirable. The total observation times were 31.1 hrs at 307 gm, 270 hrs at 616 gm and 850 hrs at 1033 gm. The observed number of bursts with more than 1000 particles is $\sim$ 20 at 307 gm and 616 gm and $\sim$ 10 at sea level. Furthermore the possibility of confusing some small bursts with background introduces a systematic error whose importance increases with altitude. The ionization chamber records the background ionization as a continuous straight line with a slope slightly different from zero at sea level, on which the bursts are observed as small vertical jumps. As one goes up in the atmosphere the background ionization and consequently the slope of the straight line increases; thus, as shown schematically below, it becomes increasingly difficult to distinguish

the smallest observable bursts from the accidental wiggles due to statistical fluctuations of the background ionization, this being especially true for the airplane data where the motion of the plane is another cause for accidental wiggles. In such ambiguous cases, the tendency of all

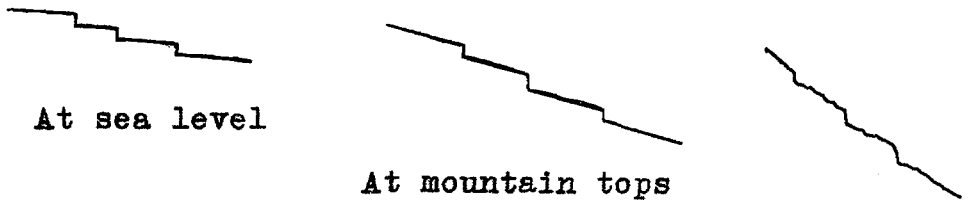

experimenters, understandably, seems to be in the direction of under-estimating the number of smallest size bursts (See Ref. 1,4). We therefore expect the observed frequency of these bursts to be too low by an unknown amount.

In converting the ionization as observed in ion-pairs to the number of particles responsible for it, the conventional value of 60 ion-pairs per cm per atmosphere of air is used. This value was taken from Swann's measurements of the ionization produced by cosmic rays in traversing a cylindrical high pressure (5 atms of argon) chamber (Ref. 39). A semi-theoretical justification can be given by computing the energy loss of a high energy electron (e.g.

by means of the formula given by Bethe (Ref. 40)) and converting it into ion-pairs, using for the effective ionization potential I and the energy spent per ion-pair ω that go into such a calculation the experimental values obtained by Segre and Bakker (Ref. 41) for 340 Mev protons. Thus one finds with I = 80 ev and ω = 33.3 ev/ion-pair, exactly 60 ion-pairs per cm path of air at 1 atm. and 20°C for an electron of total energy E = 1.7 Mev (minimum ionization) and 63 ion-pairs for an electron of energy E = 10 Mev. As the electrons responsible for bursts, being shower particles at or near the maximum development have mostly energies in the region 1 - 10 Mev, the conventional value of 60 ion-pairs seems satisfactory.

In presenting the data care was taken to follow the remark made by Christy and Kusaka (See Ref. 1, footnote 5) to the effect that a burst observed to have S particles actually has a number of particles between two limits enclosing S which are determined by the accuracy of the reading, so that in obtaining an integral distribution the lower limit must be substituted for S.

The cumulative data are shown in Tables 11, 12 and 13 for the altitudes of 307 gm, 616 gm and 1033 gm respectively. In the first four columns are listed the observed number of bursts with more than S particles and their

resulting frequency both per hour and per sec cm^2. The observed bursts (to be denoted by O) are the sum total of shield bursts (N), air bursts (H) and μ-bursts (M). To study the altitude dependence and the size-frequency distribution of shield bursts we must separate them from others. In Tables 12 and 13, the fifth column gives the frequency per cm^2 sec corrected for μ-bursts by a method explained in section 13; the μ-correction to 307 gm data is negligible. Finally the last column in each table gives the frequency per cm^2 sec of shield bursts obtained from the preceding column by subtracting the air bursts as given in fig. 13.

Table 11 (t = 307 gm)

S	No of Observed bursts	O(>S) per hr	O(>S) per sec cm^2	N(>S) per cm^2 sec
310	45	1.45	2.21×10^{-6}	2.18×10^{-6}
520	40	1.29	1.96	1.89
730	27	0.87	1.32	1.26
935	24	0.77	1.17	1.10
1140	22	0.71	1.08	1.00
1350	18	0.58	0.88	0.81
1550	12	0.39	0.59	0.54
1770	8	0.26	0.39	0.35
2080	7	0.23	0.35	0.31

Table 12 (t = 616 gm)

S	No of Ob. Bursts	O(>S) per hr	O(>S) per cm^2 sec	O-M(>S)	N(>S)
235	140	0.52	7.91×10^{-7}	7.35×10^{-7}	7.21×10^{-7}
465	66	0.24	3.65	3.51	3.40
935	28	0.10	1.52	1.49	1.40
1860	10	0.027	0.41	0.40	0.36

Table 13 (t = 1033 gm)

S	No of Ob. Bursts	O(>S) per hr	O(>S) per cm^2 sec	O-M(>S)	N(>S)
235	80	0.093	1.41×10^{-7}	1.00×10^{-7}	0.98×10^{-7}
465	29	0.033	0.50	0.38	0.37
935	12	0.013	0.20	0.17	0.16
1860	4	0.004	0.06	0.054	0.048

The data for N(>S) are plotted in figs. 14, 15, 16. The indicated errors are standard deviations and do not include systematic errors. In each case a straight line is drawn through the experimental points which passes above the point for the smallest size burst as this point is presumed to be somewhat underestimated. The slope of the line is found to be -1.75 ∓ 0.20 at sea level, -1.54 ∓ 0.15 at 616 gm and -1.14 ∓ 0.20 at 307 gm (30,000 feet); the errors being composites of the statistical errors and the theoretical uncertainties in the μ-burst estimates.

According to section 3.b the shape of the size-frequency distribution of the shield bursts should reflect quite closely the shape of the integral spectrum of the primary particles. Hence the observed change with altitude in the slope of the size-frequency distribution disagrees with our assumption of a simple exponential absorption of the primary spectrum. This discrepancy indicates the existence of another agent for producing shield bursts. The most likely cause would be the secondary particles that come out of meson-producing collisions in the air, mainly charged π -mesons and perhaps some high energy nucleons whose effects are neglected in our analysis. These may well account for a part of the shield bursts whose relative importance increases with altitude; though it is not possible to make a quantitative estimate at present. Some experimental evidence in favor of such a hypothesis can be drawn from burst experiments with chambers screened by coincidence circuits. By excluding the bursts accompanied by air showers both Fahy and Stinchcomb obtained at 3500 m (675 gm) a size-frequency distribution that has a slope of -2, which would correspond to an inverse cube law for the primary differential spectrum as we have assumed. But when the bursts accompanied by air showers are added

to the previous data, the slope becomes -1.8. Furthermore the bursts accompanied by air showers are shown to be mainly due to the penetrating component (See section 10).

We might also note that at sea level Lapp obtained the same inverse square law with a similar counter-chamber arrangement to exclude air showers. As the μ-bursts are expected to give an inverse square distribution, this fact is additional evidence for assuming a primary differential spectrum of the form $P_o \frac{dE}{E^3}$.

13. Remarks on μ-bursts

A theoretical size-frequency distribution for μ-bursts at sea level was computed by Christy and Kusaka (Ref. 1). We have used their results after applying the following corrections:

1) In C - K's calculations the mass of the μ-meson was taken as $m_\mu = 177\ m_e$ and the total intensity of the μ-meson beam at sea level as $I = 1.00 \times 10^{-2}$ cm^{-2} sec^{-1} $sterad^{-1}$. We changed these figures to $m_\mu = 215\ m_e$ as given by Brode (Ref. 42) and $I = 0.83 \times 10^{-2}$ cm^{-2} sec^{-1} $sterad^{-1}$ as given by Rossi (Ref. 28).

2) C - K used the "completely screened" value for

the shower unit in lead (i.e. 5.9 gm/cm^2) We changed it to 7.5 gm/cm^2; this, by extending the effective burst range, increases the burst rate by a factor of $\frac{7.5}{5.9} = 1.27$.

3) The effect of fluctuations seems to have been over-estimated by C - K. At that time the preliminary calculations of Nordsieck, Lamb and Uhlenbeck (Ref. 43) had shown that the dispersion σ (defined by $\sigma^2 = (s^2)_{Av} - (S_{Av})^2$) is of the order of $\frac{1}{2} S_{Av}$ near the maximum of the shower. As the approximate Furry model (Ref. 44) gives a dispersion of $\sigma \sim S_{Av}$ while the classical Poisson distribution gives only $\sigma \sim S^{1/2}$, C - K concluded that near the maximum of the shower where the largest contribution to bursts arises the actual fluctuations would be better approximated by the Furry model; the result of using this model was an increase of the burst rate by a factor of 1.5. Later, however, Scott and Uhlenbeck (Ref. 45) improved their early calculations and reduced their estimate for σ to only a few times the Poisson value; therefore it seems now that a better approximation to the actual burst rate will be obtained by completely neglecting the fluctuations. The same conclusion is drawn by Belenky (Ref. 46) from Landau's unpublished calculations.

The results of C - K with the indicated modifications are listed in Table 14 below and plotted in fig. 17, in

burst per cm^2 sec, where β is in ev.

Table 14

βS	Bremsstrahlung bursts	Knock-on bursts	Total bursts
2×10^9	5.71×10^{-8}	0.86×10^{-8}	6.57×10^{-8}
4	1.81×10^{-8}	0.16×10^{-8}	1.97×10^{-8}
8	0.48×10^{-8}	2.58×10^{-10}	5.04×10^{-9}
16	1.20×10^{-9}	3.87×10^{-11}	1.24×10^{-9}
32	2.43×10^{-10}	5.74×10^{-12}	2.49×10^{-10}

To obtain the burst rate at t = 616 gm we may assume that the high energy mesons responsible for bursts are formed very high up in the atmosphere so that the difference between the meson spectra at 616 gm and at 1033 gm is solely due to the absorption through ionization loss and decay. At sea level C - K used a differential spectrum of the form

$$N(E)\, dE\, d\Omega = \frac{dE\, d\Omega}{\left(E + \frac{1.8}{\cos\theta}\right)^3} \qquad (13.1)$$

in which 1.8 Bev corresponds to the energy loss throughout the atmosphere. If we take the energy loss between 616 gm and 1033 gm to be 0.8 Bev (for a meson of energy $\sim$ 10 Bev) and denote by $\frac{\omega(1033)}{\omega(616)}$ the survival probability for a meson of energy E in going from 616 gm to 1033 gm along a path making an angle θ with the vertical, we

obtain at 616 gm a spectrum of the form

$$N(E)\,dE\,d\Omega = \frac{dE\;d\Omega}{\left(E+\frac{1}{\cos\theta}\right)^3}\;\;\frac{\omega(616)}{\omega(1033)} \qquad (13.2)$$

Assuming an exponential atmosphere and a linear variation of momentum with path length one easily finds,

$$\frac{\omega(616)}{\omega(1033)} = \left[\frac{1033\left(p+\frac{0.8}{\cos\theta}\right)}{616\,p}\right]^{\frac{1.3}{p\cos\theta+2}} = \left[1.68\left(1+\frac{0.8}{p\cos\theta}\right)\right]^{\frac{1.3}{p\cos\theta+2}} \qquad (13.3)$$

where p is the momentum corresponding to E(ie. pc $\cong$ E). The effect of using the spectrum (13.2) on the final burst rate may be estimated by calculating the following ratio

$$f = \frac{\int_0^{\frac{\pi}{2}} \frac{\sin\theta\,d\theta}{(\bar{E}+\sec\theta)^2}\left[1.68\left(1+\frac{0.8}{\bar{p}\cos\theta}\right)\right]^{\frac{1.3}{\bar{p}\cos\theta+2}}}{\int_0^{\frac{\pi}{2}} \frac{\sin\theta\,d\theta}{(\bar{E}+1.8\sec\theta)^2}}$$

where $\bar{E}$ is now the effective energy for producing a burst of size larger than S (as given by $\bar{E} = 6\beta S$) and for this reason the denominators are only squared. The results for the Neher chamber and for the values of S needed in section 11 are listed below in Table 15.

Table 15

S	$\bar{E}$ in Bev	f	M_{1033} in $cm^{-2}sec^{-1}$	M_{616} in $cm^{-2}sec^{-1}$
235	16	1.34	0.415×10^{-7}	0.56×10^{-7}
465	31	1.20	0.12×10^{-7}	0.142×10^{-7}
935	63	1.10	0.29×10^{-8}	0.32×10^{-8}
1860	126	1.05	0.61×10^{-9}	0.695×10^{-9}

In computing the energies of the second column we have used $\beta = 11.3$ Mev. The slight difference from $\beta = 10.2$ Mev as deduced in section 2 is due to the presence of a steel wall between the lead shield and ion chamber (inner wall). This wall introduces a transition effect for the electron showers traversing it; as the critical energy for iron is larger than that for lead, the number of electrons absorbed in passing through the iron wall is larger than the number created therein. According to the estimate of Christy and Kusaka one can take care of this absorption by multiplying by 1.5 for a wall 1.5 cm thick. We shall change this estimate slightly as suggested by the more recent analyses (See Ref. 4 and Ref. 33) and take the factor as 1.6; then by assuming an exponential absorption in

the iron wall to interpolate from 1.5 cm to 0.33 cm we obtain 1.11 for the absorption factor in Neher's chamber which finally gives $\beta_{\text{Neher}} =$ 10.2 x 1.11 = 11.3 Mev. The figures in the fourth column are taken from Fig. 17 and those in the last column are obtained by multiplying together the corresponding figures in the third and fourth columns.

We have used these figures in correcting the data of Neher-Biehl for μ-bursts. It must be mentioned however that these theoretical figures may be wrong by as much as a factor of 2 when applied to a specific ion chamber because of an unknown sensitivity factor peculiar to every chamber. As it was already pointed out by Schein-Gill (Ref. 2), for apparently unaccountable experimental reasons different meters even though located at the same place record different burst rates. Recently Stinchcomb (Ref. 58) found a difference up to a factor of 2 between the burst rates recorded by the three Carnegie Model C meters that he used.

14. Mean free paths in lead

In his burst experiments at Climax, Fahy has varied the thickness of the lead shield surrounding the Carnegie meter (Ref. 33). He found a general decrease in the burst rate by a factor of 1.6 ∓ 0.06 for an increase in shield thickness from 10.7 cm to 26.7 cm. This factor was independent of burst size in the range $S = 200 - 2000$. As such an absorption is predicted in our expression (3.8) we shall use this experiment to deduce the absorption mean free path in lead λ_A of the primary radiation. A similar analysis was already made by Fahy.

As the chamber was screened against air showers by means of a coincidence counting arrangement, the bursts observed by Fahy include mainly shield bursts with a few μ-bursts. We have therefore

$$\frac{(N+M)_{10.7}}{(N+M)_{26.7}} = 1.6 \tag{14.1}$$

According to (3.8), N-bursts are exponentially absorbed:

$$N_{26.7} = N_{10.7}\ e^{-\frac{\Delta a}{\lambda_A}} = N_{10.7}\ e^{-\frac{182}{\lambda_A}} \tag{14.2}$$

where $\Delta a = 182$ gm is the difference in the effective shield thickness derived by means of the Table 6.

The absorption of μ-mesons in going through 182 gm

of lead can be neglected as it amounts to an energy loss of $\sim$ 380 Mev = 0.38 Bev whereas the effective energy for producing bursts with S = 1000 is from Christy-Kusaka, $E = 10 \beta S = 10 \times 1.6 \times 10^7 \times 10^3 = 160$ Bev. Thus we have

$$M_{26.7} = M_{10.7} \tag{14.3}$$

Combining Fahy's experimental value of $N + M = 1.95 \times 10^{-8}$ $cm^{-2} sec^{-1}$ and the theoretical value of $M = \frac{0.138 \times 1.07}{1.18} = 0.13 \left(\times 10^{-8}\right) cm^{-2}$ sec^{-1} (derived approximately for Climax as explained in section 13) with (14.1, 2,3), one finds

$$\lambda_A = 355 \mp 55 \text{ gm/cm}^2$$

The error indicated is compounded of the uncertainties in the experimental absorption factor and the theoretical value for M. In his analysis, Fahy found $\lambda_A = 346 \mp 36$ owing mainly to his slightly different figure for M.

Since there are no reasons to the contrary in our analysis, we shall assume the equality of the absorption and collision mean free paths in lead. We then obtain

$$\lambda_c = 355 \mp 55 \text{ gm/cm}^2$$

which is about twice the geometrical mean free path (160 gm) corresponding to the geometrical cross section for collisions. In some cases it has been suggested (see

e.g. Ref. 47) that a geometrical cross section for catastrophic collisions may still give rise to an absorption length of $\sim$ 300 gm by means of a cascade process. However in burst experiments where the detection scheme is so heavily energy sensitive, the effect of the secondary nucleons will be negligible owing to their strong energy degeneration. The possibly larger effect of the secondary π-mesons was already taken care of in 3.d and shown to be in fact quite small.

Our value for the absorption mean free path agrees with the results of several authors (See Ref. 48) on the absorption of star-producing and penetrating shower producing radiations. On the other hand, our collision mean free path disagrees with the results of Cocconi (Ref. 49) and Sitte (Ref. 50) who found $\sim$ 160 gm for the interaction mean free path in lead of the penetrating shower producing radiation. It does agree though with an extrapolation of the Berkeley results on the collision cross sections of high energy neutrons in various materials. By varying the neutron energy from 90 Mev up to 270 Mev, DeJuren and Moyer found that the total cross section (which includes the effect of "shadow scattering") for each material drops rapidly between 100 and 180 Mev to a level which continues with little further variation up to 270 Mev (Ref. 51).

The result for lead at 270 Mev is $\sigma_{total} = 2.84$ barnes. Also DeJuren (Ref. 52) by means of a "poor geometry" arrangement measured the inelastic collision cross section (which may be somewhat lower than the actual one) and found that $\frac{\sigma_{in}}{\sigma_{tot}} = 0.50$ for 270 Mev neutrons on lead. Combining the two values for 270 Mev, one obtains $\lambda_c =$ 242 gm/cm^2 for lead. An increase from 242 to 355 would be reasonable considering the large gap between the two energy regions.

15. Mean free paths in air

To obtain the altitude variation of shield bursts we have plotted in fig. 18 the points for S = 500, 1000 and 1500 derived from Neher-Biehl data at 307 gm, 616 gm and 1033 gm. The errors are compounded of the statistical errors and the theoretical uncertainty in the μ-burst estimates, but are still somewhat arbitrary. The uncertainty in the μ-burst estimate affects mostly the sea level data. The straight line (dashed in fig. 18) that joins the three points for S = 1000 gives $t_{int} = 159$ gm for the absorption length of the integrated intensity. From fig. 19 we see that an approximately exponential variation between 300 gm and 1000 gm with an apparent $t_{int} = 159$ gm can be obtained after the Gross transformation if we assume

$t_A = 185$ gm. Similarly the points for S = 500 give $t_A = 200$ gm and those for S = 1500 give $t_A = 175$ gm. The observed discrepancy in the values of t_A for different burst sizes is a reflection of the fact that the size-frequency distributions at different altitudes do not have exactly the same shape. We adopt a final value of

$$t_A = 185 \mp 20 \text{ gm/cm}^2$$

For the collision mean free path in air we shall assume the same value $t_c = 185 \mp 20$ gm/cm^2, as we did in lead. The collision cross section thus found is consistent with the results of Berkeley experiments (see section 14) with high energy neutrons from which a collision mean free path of 142 gm/cm^2 for 270 Mev neutrons in air can be deduced. However, contrary to the case for lead, the value for the absorption mean free path does not agree with that obtained by several observers for the star-producing and penetrating shower producing radiations which is around 120 - 140 gm/cm^2 (See e.g. Ref. 48). It is especially difficult to reconciliate it with the values of $t_A = 124 \mp 8$ gm given by Fahy for the absorption of bursts between 3500 m (675 gm) and sea level or $t_A = 65 \mp 14$ gm given by Stinchcomb for the absorption between the top of the atmosphere and 3500 m or $t_A = 125 \mp 8$ gm and $t_A = 135 \mp 11$ given

by Rossi et al (Ref. 31) for the absorption between 383 gm and 273 gm of bursts containing more than $\sim$ 100 particles at the respective latitudes of 55° N and 20° N. Perhaps all one can do is to point out the general disagreement that exists between the other observers as well.

16. Primary spectrum

To compare the theoretical burst rate as given by (3.8) with the data, we have to know the spectrum and intensity of the primary radiation. We have seen that the shape of the size-frequency distribution reflects the shape of the primary spectrum quite closely (See 3b), so that we must have

$$f(E)\,dE = \frac{P_0}{E^3}\,dE \qquad \text{for} \quad E \gtrsim 80 \text{ Bev}.$$

For smaller energies we have the information obtained by Millikan and his collaborators in ionization measurements throughout the atmosphere at several latitudes (see e.g. Janossy's book, Ref. 53). According to Neher the results suggest a differential primary spectrum of $\frac{P}{E^{2.53}}\,dE$ in the range 10 Bev $\leq E \leq$ 20 Bev. The same experiments give also the total intensity of the primary radiation entering the atmosphere. According to Neher's recent reappraisal of the data (Ref. 54), the total vertical intensity at the

equator is I = 0.012 particles/cm^2 sec sterad. The simplest way to combine these informations is to assume

$$f(E)dE = \left(\frac{\alpha_1}{E}\right)^{1.53} \frac{dE}{E} \qquad for \quad 12.6 \leq E \leq 20 \text{ Bev}.$$

and

$$f(E)\,dE = \left(\frac{\alpha_2}{E}\right)^{2} \frac{dE}{E} \qquad for \quad 20 \leq E$$

where α_1 , α_2 are to be determined from the continuity condition

$$\left(\frac{\alpha_1}{20}\right)^{1.53} = \left(\frac{\alpha_2}{20}\right)^{2}$$

and the total intensity relation

$$I = 0.012 = \int_{12.6}^{20} \left(\frac{\alpha_1}{E}\right)^{1.53} \frac{dE}{E} + \int_{20}^{\infty} \left(\frac{\alpha_2}{E}\right)^{2} \frac{dE}{E}$$

and where 12.6 Bev is the minimum energy of the protons arriving to the equator and is different from the usual value of 15 Bev because of a correction due to the tilt between the earth's axis and the magnetic dipole (See Ref. 53). One thus obtains,

$$f(E)dE = \frac{4.1}{E^3}\, dE \qquad \text{per cm}^2 \text{ sec sterad}$$

(where E is in Bev)

near the vertical at the top of the atmosphere. It must be mentioned that Van Allen and Singer's more direct measurements of the primary intensity at the top of the atmosphere by means of G-M counter telescopes placed in rockets gave

results disagreeing with ionization results by a factor of 2 (See e.g. Ref. 55, 56). Van Allen's latest value at the equator is $I = 0.024$. However the counter results may be too high due to the atmospheric albedo which is difficult to account for completely. The ionization results on the other hand must be increased by about 20% to take into account the energy lost in the form of neutrinos. In our case there is another factor which about compensates this increase. It has been found that only 80% of the primary cosmic radiation consists of protons, the remainder being made up of heavier nuclei, mainly α-particles. (See e.g. Ref. 57). According to Bradt and Peters the heavy particles have a collision cross section very close to the geometrical one; they should therefore be absorbed in the air much more rapidly than the protons and consequently only 80% of the total incoming intensity would be effective in producing the observed bursts. Thus we shall adopt the spectrum $f(E)dE = \frac{4.1}{E^{\delta}}\, dE$ without any corrections with the understanding that it may be too low by 50%.

17. Comparison of the theoretical burst rate with the data of Neher-Biehl

Substitution in (3.8) of the values for P_0, λ_A, λ_c, α, $\tilde{x}_{1(s)}$, $M(s)$, β and multiplication by 1.14 for secondary

interactions give for S = 500, 1000, 1500,

$$N(>500) = 7.28 \times 10^{-4} \; J\,(t/t_A) \quad cm^{-2}\,sec^{-1}.$$
$$N(>1000) = 1.7 \times 10^{-5} \; J\,(t/t_A) \quad cm^{-2}\,sec^{-1}. \qquad (17.1)$$
$$N(>1500) = 7.74 \times 10^{-6} \; J\,(t/t_A) \quad cm^{-2}\,sec^{-1}.$$

From the experimental points for the corresponding burst sizes it was found in section 15 that $t_A = 200$ for $S = 500$, $t_A = 185$ for $S = 1000$ and $t_A = 175$ for $S = 1500$. Substituting these values in (17.1) and using fig. 19 we derive the theoretical burst rates for various altitudes and burst sizes. The results are shown in fig. 18 where the experimental points are joined by dashed lines while the theoretical points are joined by full curves. The theoretical and experimental points agree quite well for $S = 1000$; for $S = 500$ the theoretical curve lies higher by a factor of 2 and for $S = 1500$ it lies lower by a factor of 1.5. This variation with S is a consequence of the non-identical shapes of the experimental size-frequency distributions at three altitudes. It shows that we cannot use this data to obtain some confirmation or refutation for the value of any of the quantities used in our analysis without subtracting first the bursts due to secondary particles. However it is evident that there is agreement as to the order of magnitude in the whole interval $400 \leqslant S \leqslant 1600$.

18. Summary of conclusions

The production of photons through the intermediary of short-lived neutral mesons in collisions of primary protons with shield nuclei is shown to be a process capable of explaining the bulk of the high-altitude bursts of size S = 400 - 1000 observed under thick absorbers. The absolute burst rate predicted according to the neutral meson hypothesis, by assuming a primary differential spectrum in the form $f(E)dE = \frac{4.1}{E^3} dE$ particles per cm^2 sec sterad, an exponential absorption in the air with a mean free path of 185 ∓ 20 gm/cm^2 and a collision-absorption mean free path in lead of 355 ∓ 55 gm/cm^2 agrees within experimental errors with the burst rate found by Neher-Biehl. The absorption mean free path in air is deduced from the data of Neher-Biehl while that in lead is deduced from Fahy's data. The form of the primary spectrum is chosen so as to agree with the results of counter-chamber coincidence experments by Lapp, Fahy and Stinchcomb; its absolute value is derived from the ionization measurements of Millikan and his collaborators. The contribution of the soft component of air showers is estimated to be negligible at all altitudes while that of μ-mesons is significant only at sea level.

On the other hand, the experimental size-frequency

distributions at three altitudes do not agree with each other if one attributes all shield bursts to primary protons, which are absorbed exponentially throughout the atmosphere. A fraction of the high altitude bursts must therefore be due to secondary particles, presumably charged π-mesons and secondary nucleons. A quantitative estimate of this fraction is not available at present, partly because of the lack of statistical accuracy in the data and partly because of the lack of detailed knowledge about the primary interaction.

References

1. R. F. Christy and S. Kusaka; Phys. Rev. 59, 414 (1941).
2. M. Schein and P. S. Gill; Rev. of Mod. Phys. 11, 267 (1939).
3. M. Schein and R. E. Lapp; Phys. Rev. 65, 63 (1944).
4. R. E. Lapp; Phys. Rev. 69, 321 (1946).
5. H. Bridge, B. Rossi and R. Williams; Phys. Rev. 72, 259 (1947).
6. H. Bridge, W. E. Hazen and B. Rossi; Phys. Rev. 73, 179 (1948).
7. Bjorklund, Crandall, Moyer and York; Phys. Rev. 77, 213 (1950).
8. J. Steinberger, W. K. H. Panofsky and J. Steller; Phys. Rev. 78, 802 (1950).
9. H. L. Bradt, M. F. Kaplon and B. Peters; Hel. Phys. Acta XXIII, 24 (1950).
10. Camerini, Fowler, Lock and Muirhead; Phil. Mag. 41, 413 (1950).
11. J. J. Lord, J. Fainberg and M. Schein; Phys. Rev. 80, 970 (1950).
12. E. Fermi; Prog. Theor. Phys. 5, 570 (1950).
13. W. Heitler and L. Jánossy; Hel. Phys. Acta. XXIII, 417 (1950).
14. M. F. Kaplon, B. Peters and H. L. Bradt; Phys. Rev. 76, 1735 (1949).
15. A. G. Carlson, J. E. Hooper and D. T. King; Phil. Mag. 41, 701 (1950).
16. H. S. Snyder; Phys. Rev. 76, 1563 (1949).

17. J. Roberg and L. W. Nordheim; Phys. Rev. 75, 444 (1949).

18. S. Belenky; J. Phys. USSR VIII, 347 (1944).

19. I. B. Bernstein; Phys. Rev. 80, 995 (1950.

20. H. A. Bethe and W. Heitler; Proc. Roy. Soc. 159, 432 (1937).

21. W. Blocker, R. W. Kennedy and W. K. H. Panofsky; Phys. Rev. 79, 419 (1950.

22. K. M. Crowe and E. Hayward; Phys. Rev. 80, 40 (1950).

23. O. Halpern and H. Hall; Phys. Rev. 73, 477 (1948).

24. S. Belenky; J. Phys. USSR VIII, 305 (1944).

25. H. Messel; Phys. Rev. 82, 259 (1951).

26. H. J. Bhabha and S. K. Chakrabarty; Phys. Rev. 74, 1312 (1948).

27. F. J. Milford and L. L. Foldy; Phys. Rev. 81, 13 (1951).

28. B. Rossi; Rev. Mod. Phys. 20, 564 (1948).

29. B. P. Gregory and J. H. Tinlot; Phys. Rev. 81, 675 (1951).

30. E. F. Fahy and M. Schein; Phys. Rev. 75, 207 (1949).

31. A. J. McMahon, B. Rossi and W. F. Burditt; Phys. Rev. 80, 157 (1950).

32. E. F. Fahy and M. Schein; Phys. Rev. 76, 170 (1949).

33. E. F. Fahy; Phys. Rev. 83, 413 (1951).

34. G. Cocconi, A. Loverdo and V. Tongiorgi; Phys. Rev. 70, 846 (1946).

35. E. Amaldi, C. Castagnoli, A. Gigli and S. Sciuti; Nuovo Cimento VII, 401 (1950).

36. B. Rossi and K. Greisen; Rev. Mod. Phys. 13, 269 (1941).

37. M. M. Mills; Thesis, California Institute of Technology 70 (1948).

38. W. Heisenberg; Cosmic Radiation, page 26, Dover, New York (1946).

39. W. F. G. Swann; Phys. Rev. 44, 961 (1933).

40. H. A. Bethe; Handbuch der Phys. 24, 1, page 523.

41. C. J. Bakker and E. Segrè; Phys. Rev. 81, 489 (1951).

42. R. B. Brode; Rev. Mod. Phys. 21, 37 (1949).

43. A. Nordsieck, W. E. Lamb, Jr. and G. E. Uhlenbeck; Physica 7, 344 (1940).

44. W. H. Furry; Phys. Rev. 52, 569 (1937).

45. W. T. Scott and G. E. Uhlenbeck; Phys. Rev. 62, 497 (1942).

46. S. Belenky; J. Phys. USSR X, 144 (1946).

47. G. Cocconi, V. Cocconi Tongiorgi and M. Vidgoff; Phys. Rev. 79, 768 (1950).

48. G. Bernardini, C. Cortini and A. Manfredini; Phys. Rev. 76, 1792 (1949).

49. G. Cocconi; Phys. Rev. 76, 984 (1949).

50. K. Sitte; Phys. Rev. 78, 714 (1950).

51. J. DeJuren and B. J. Moyer; Phys. Rev. 81, 919 (1951).

52. J. DeJuren; Phys. Rev. 80, 27 (1950).

53. L. Jánossy; Cosmic Rays, pages 293-299, Oxford, London (1950).

54. H. V. Neher; Private Communication.

55. J. A. Van Allen and A. V. Gangnes; Phys. Rev. 78 50 (1950.

56. J. A. Van Allen and S. F. Singer; Phys. Rev. 78, 819 (1950).

57. H. L. Bradt and B. Peters; Phys. Rev. 77, 54 (1950).

58. T. Stinchcomb; Phys. Rev. 83, 422 (1951).

FIGURE 1

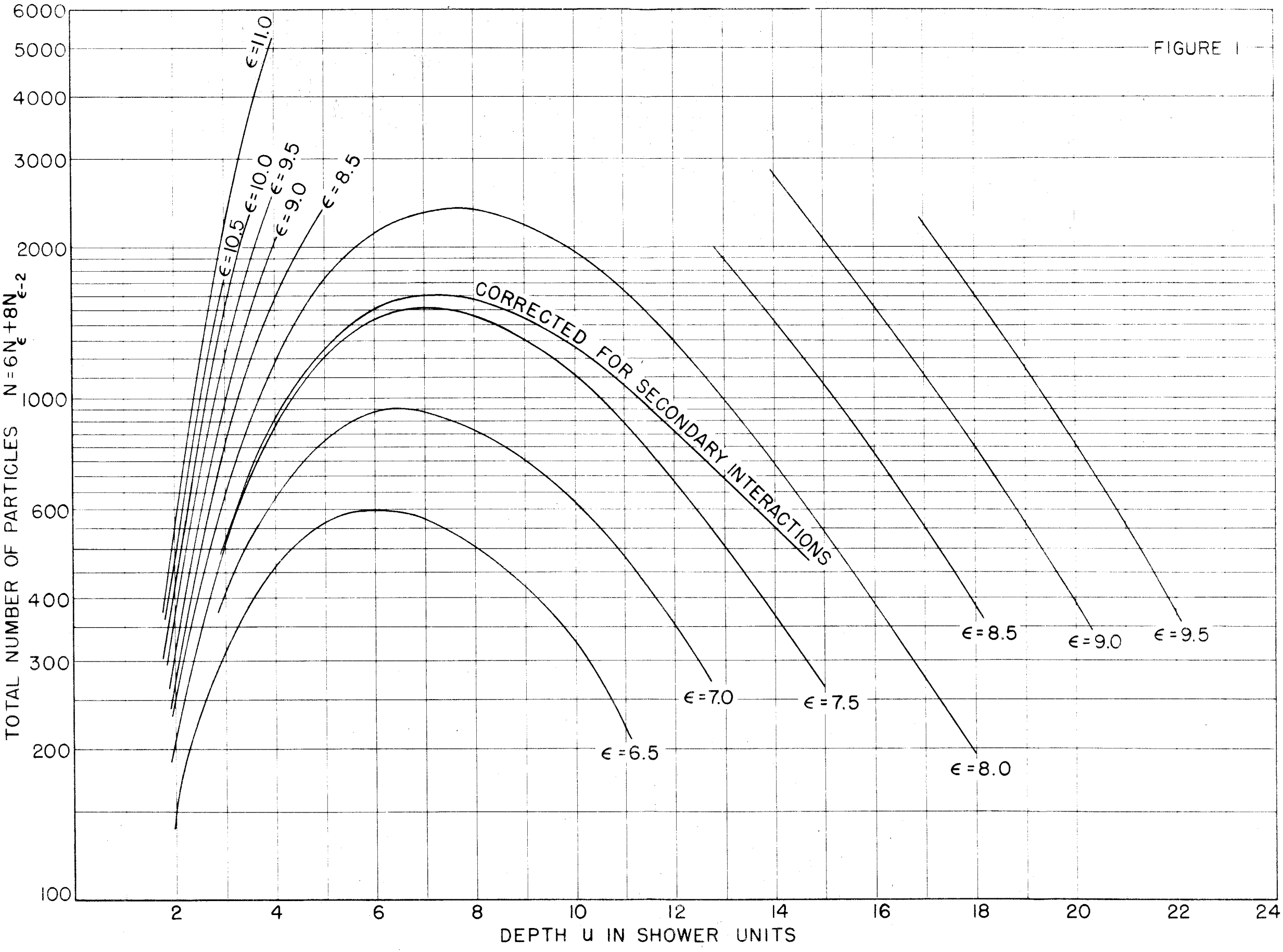
TOTAL NUMBER OF PARTICLES $\tilde{N}=6N_{\epsilon}+8N_{\epsilon-2}$
DEPTH u IN SHOWER UNITS
CORRECTED FOR SECONDARY INTERACTIONS
$\epsilon=11.0$
$\epsilon=10.5$
$\epsilon=10.0$
$\epsilon=9.5$
$\epsilon=9.0$
$\epsilon=8.5$
$\epsilon=8.0$
$\epsilon=7.5$
$\epsilon=7.0$
$\epsilon=6.5$
6000
5000
4000
3000
2000
1000
600
400
300
200
100
2
4
6
8
10
12
14
16
18
20
22
24

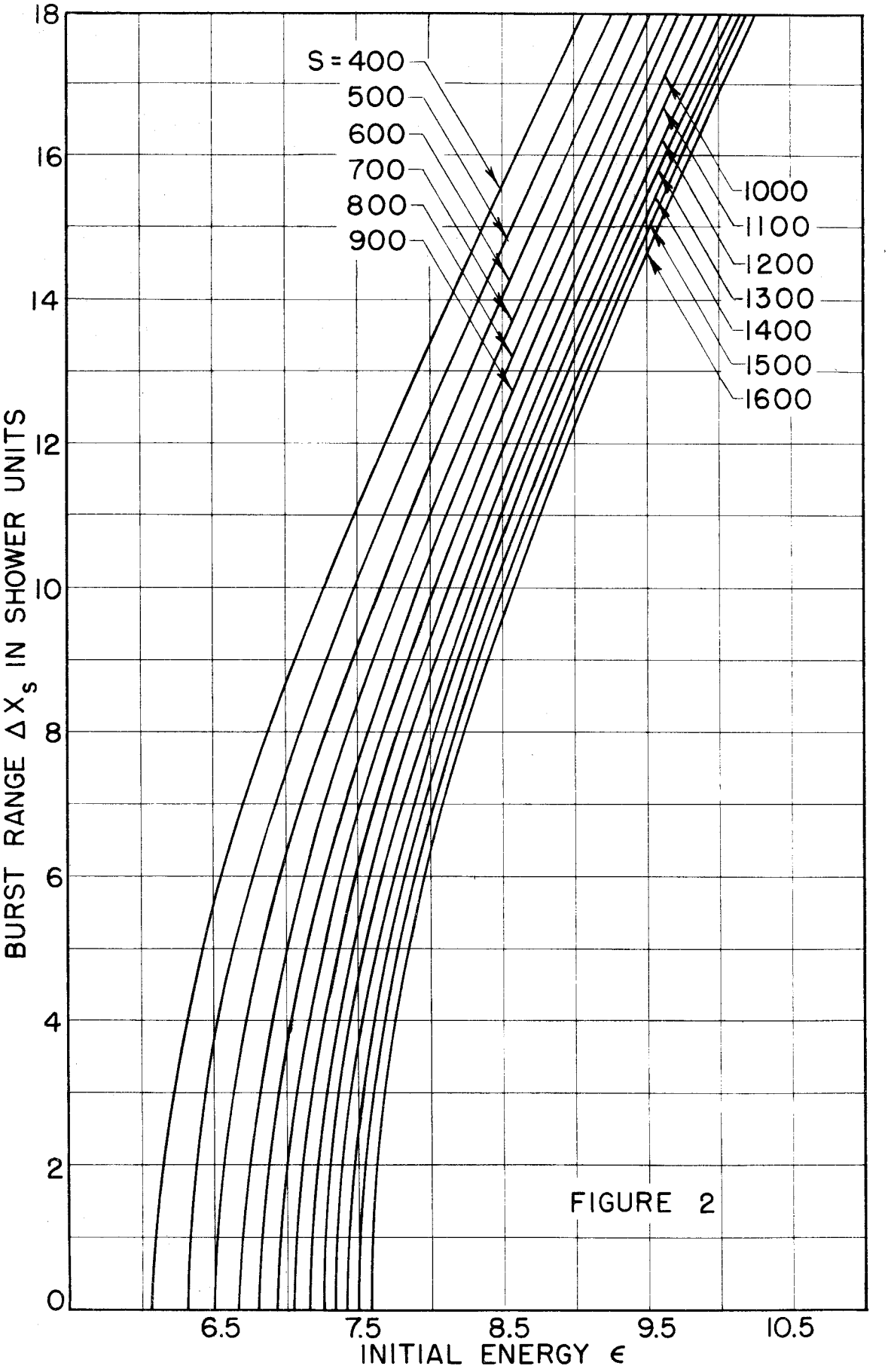
S = 400
500
600
700
800
900
1000
1100
1200
1300
1400
1500
1600
BURST RANGE ΔX_s IN SHOWER UNITS
INITIAL ENERGY ϵ
0
2
4
6
8
10
12
14
16
18
6.5
7.5
8.5
9.5
10.5

FIGURE 2

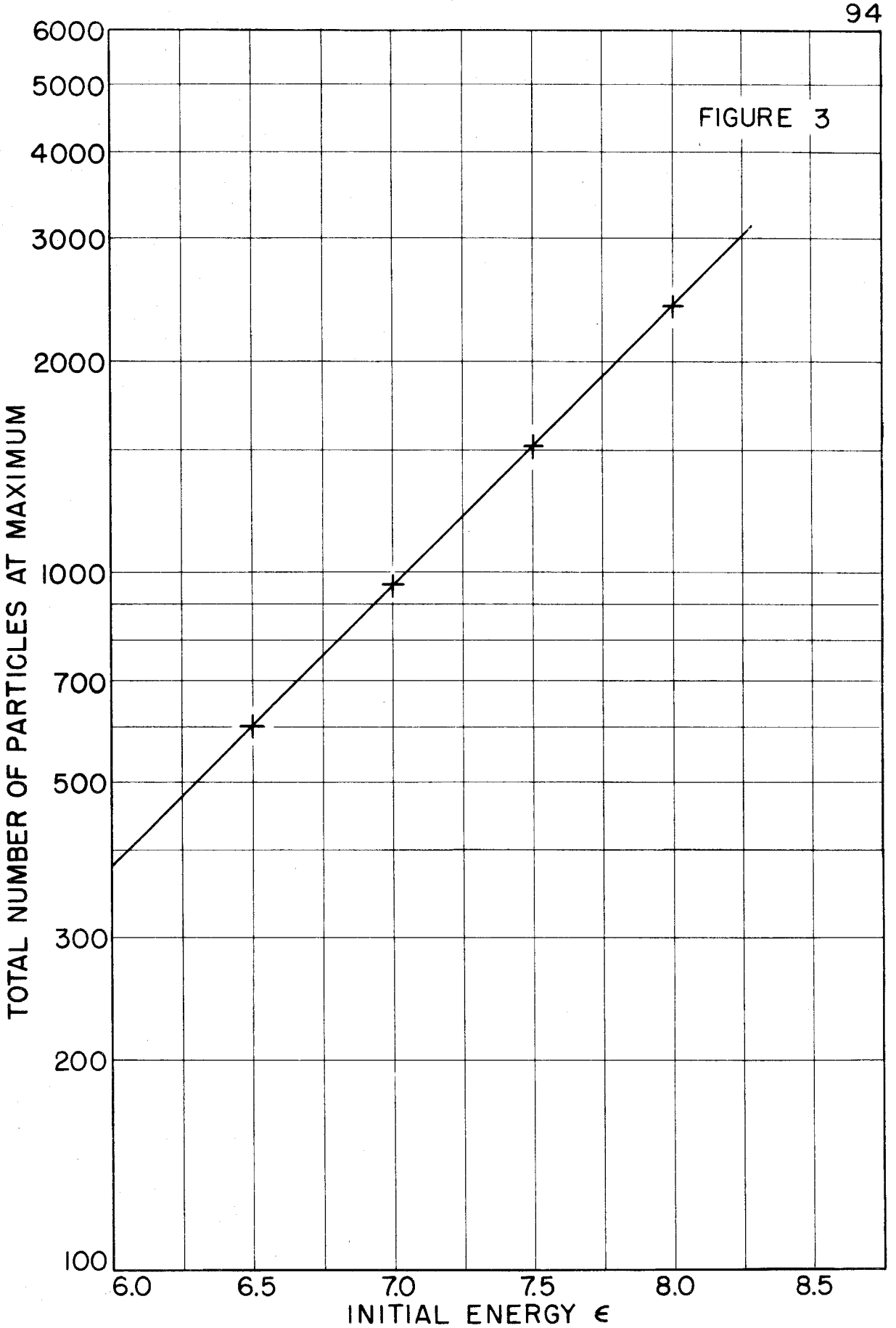
FIGURE 3
TOTAL NUMBER OF PARTICLES AT MAXIMUM
6000
5000
4000
3000
2000
1000
700
500
300
200
100
6.0
6.5
7.0
7.5
8.0
8.5
INITIAL ENERGY ϵ

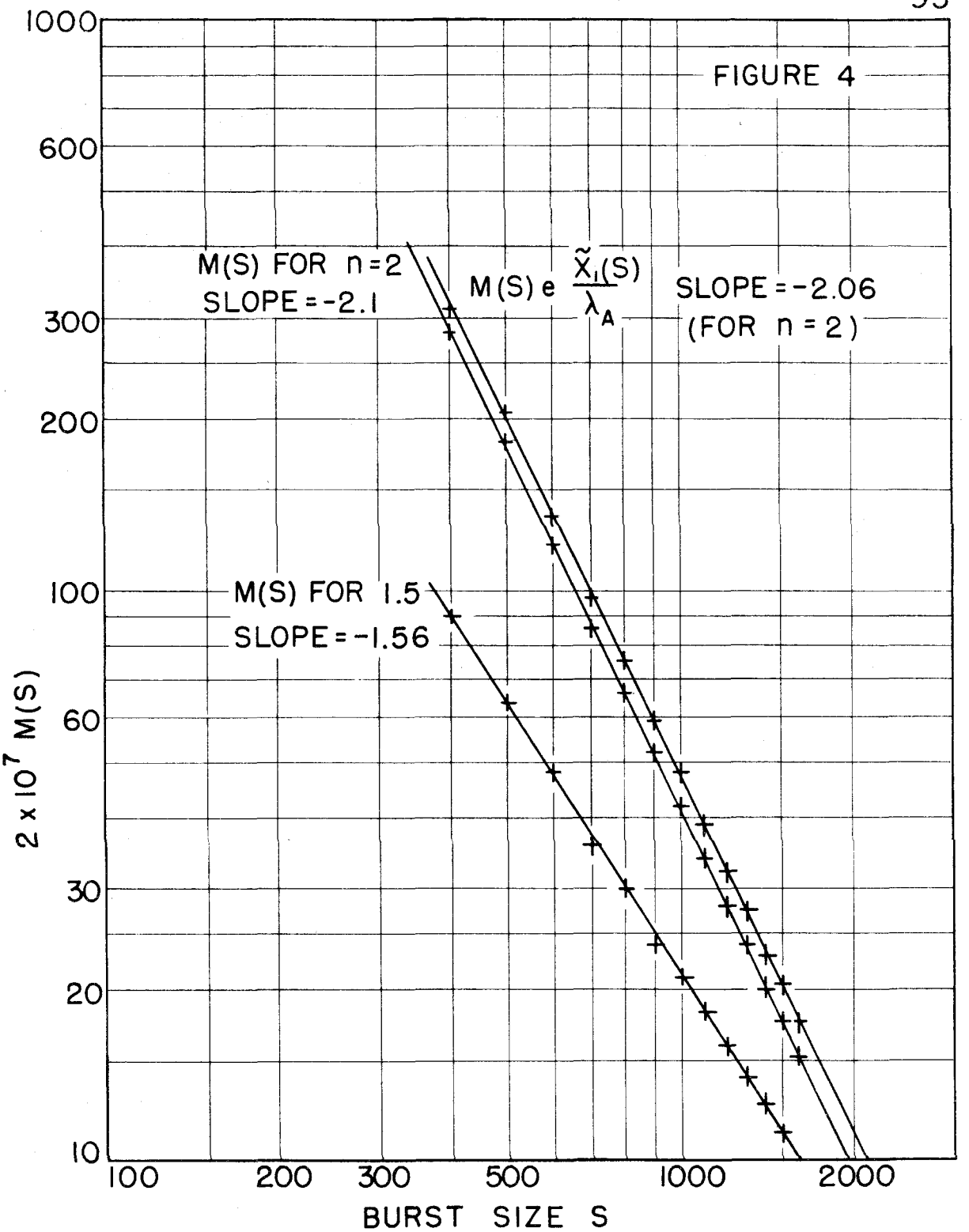
FIGURE 4
M(S) FOR n=2
SLOPE=-2.1
M(S) e $\frac{\tilde{X}_1(S)}{\lambda_A}$
SLOPE=-2.06
(FOR n=2)
M(S) FOR 1.5
SLOPE=-1.56
2 x 10^7 M(S)
1000
600
300
200
100
60
30
20
10
100
200
300
500
1000
2000
BURST SIZE S

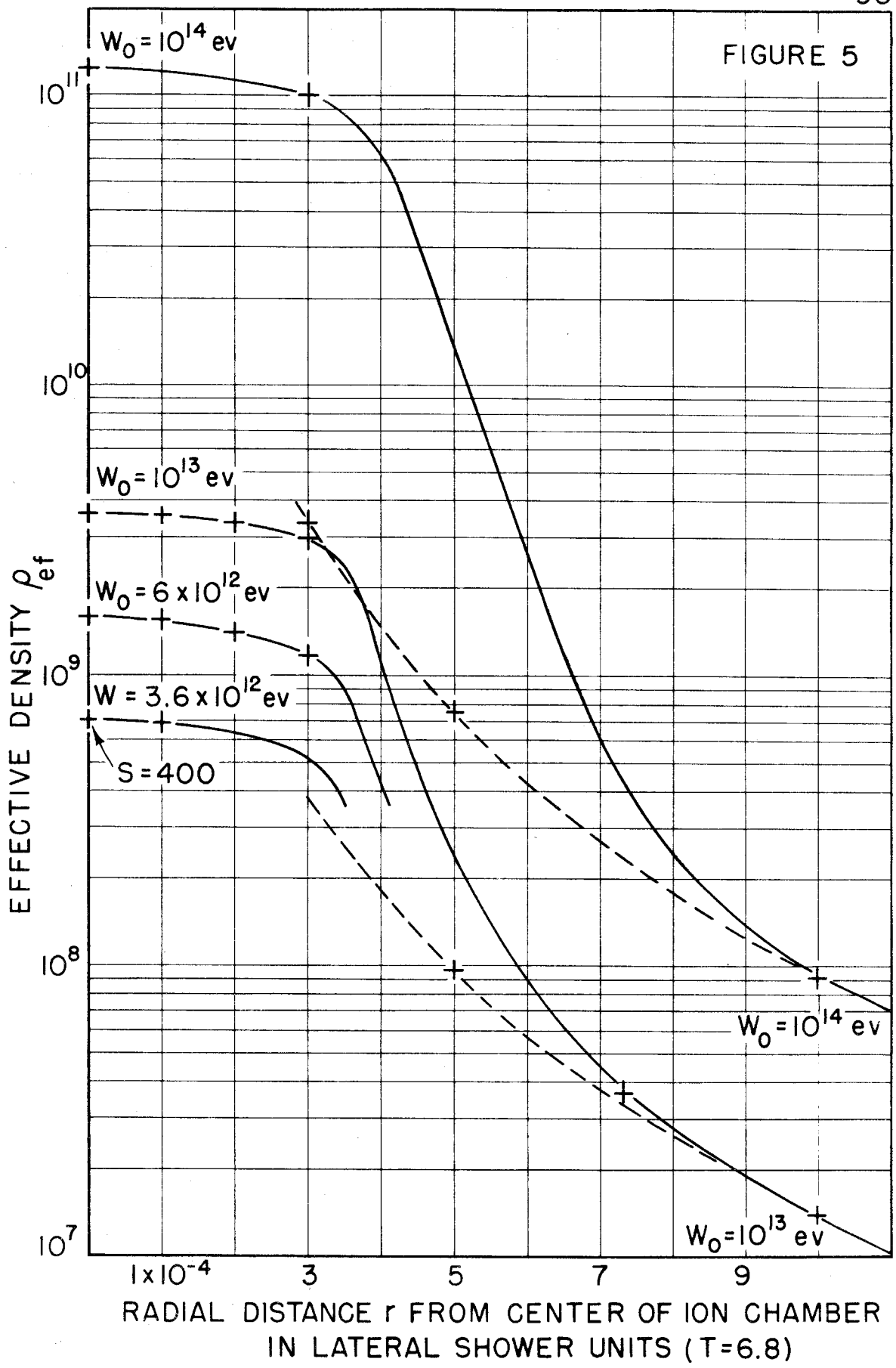
FIGURE 5
$W_0 = 10^{14}$ ev
10^{11}
10^{10}
$W_0 = 10^{13}$ ev
$W_0 = 6 \times 10^{12}$ ev
10^{9}
$W = 3.6 \times 10^{12}$ ev
S = 400
10^{8}
$W_0 = 10^{14}$ ev
10^{7}
$W_0 = 10^{13}$ ev
EFFECTIVE DENSITY ρ_{ef}
1×10^{-4}
3
5
7
9
RADIAL DISTANCE r FROM CENTER OF ION CHAMBER
IN LATERAL SHOWER UNITS (T=6.8)

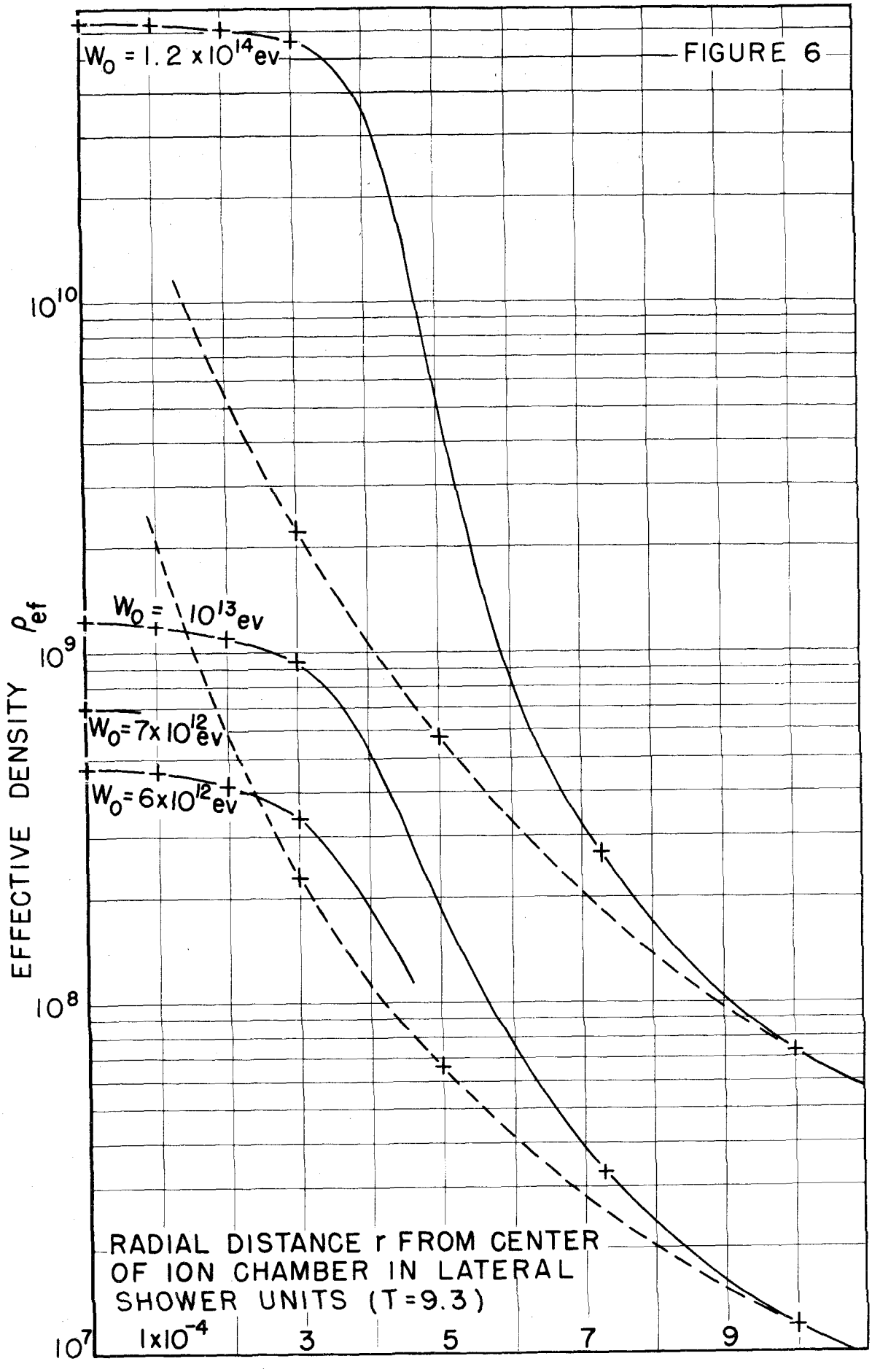
FIGURE 6
$W_0 = 1.2 \times 10^{14}$ ev
$W_0 = 10^{13}$ ev
$W_0 = 7 \times 10^{12}$ ev
$W_0 = 6 \times 10^{12}$ ev
EFFECTIVE DENSITY ρ_{ef}
10^{10}
10^{9}
10^{8}
10^{7}
RADIAL DISTANCE r FROM CENTER OF ION CHAMBER IN LATERAL SHOWER UNITS (T=9.3)
1×10^{-4}
3
5
7
9

FIGURE 7

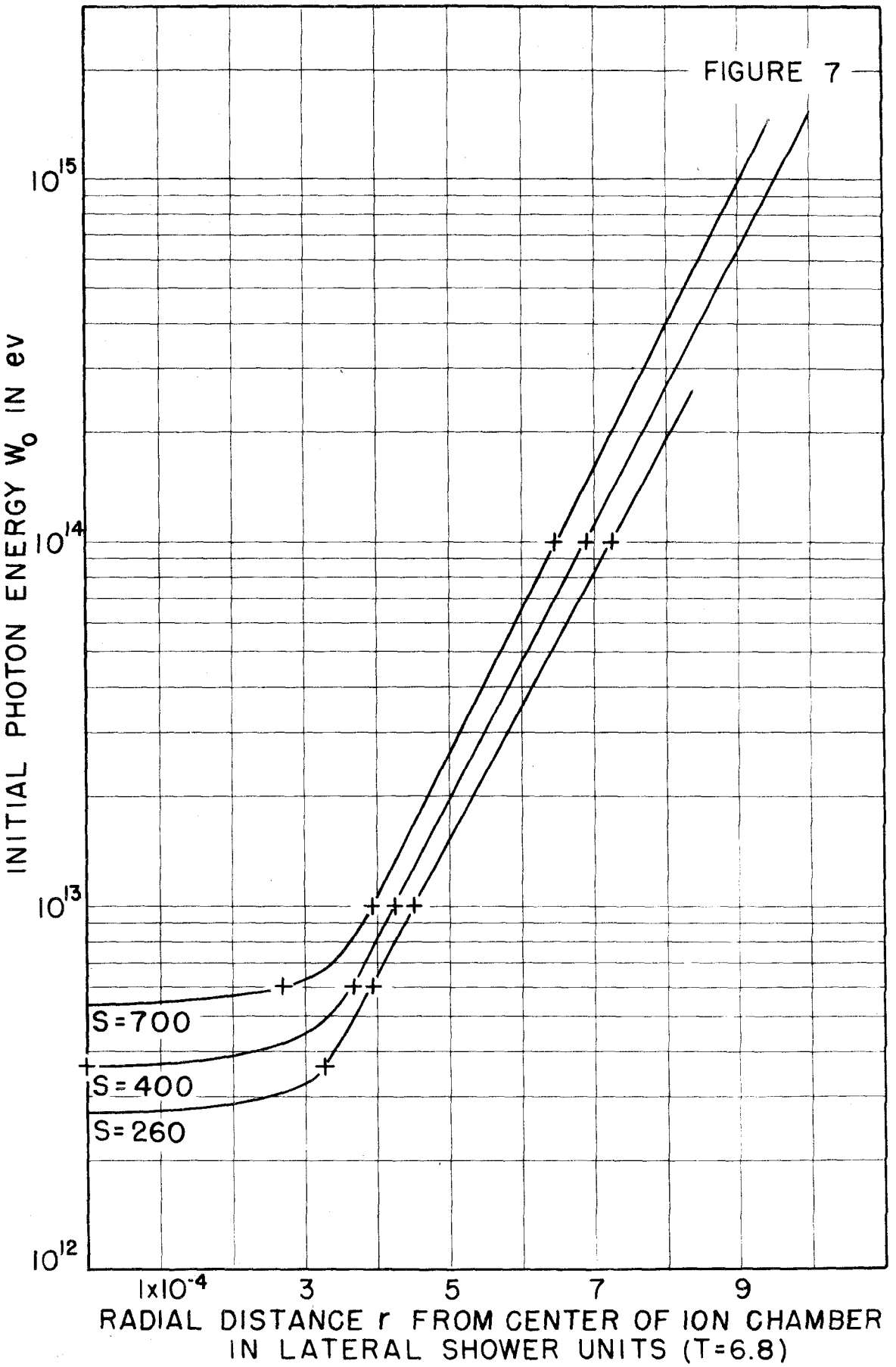
INITIAL PHOTON ENERGY W_0 IN ev
10^{15}
10^{14}
10^{13}
10^{12}
S=700
S=400
S=260
1x10^{-4}
3
5
7
9
RADIAL DISTANCE r FROM CENTER OF ION CHAMBER
IN LATERAL SHOWER UNITS (T=6.8)

FIGURE 8

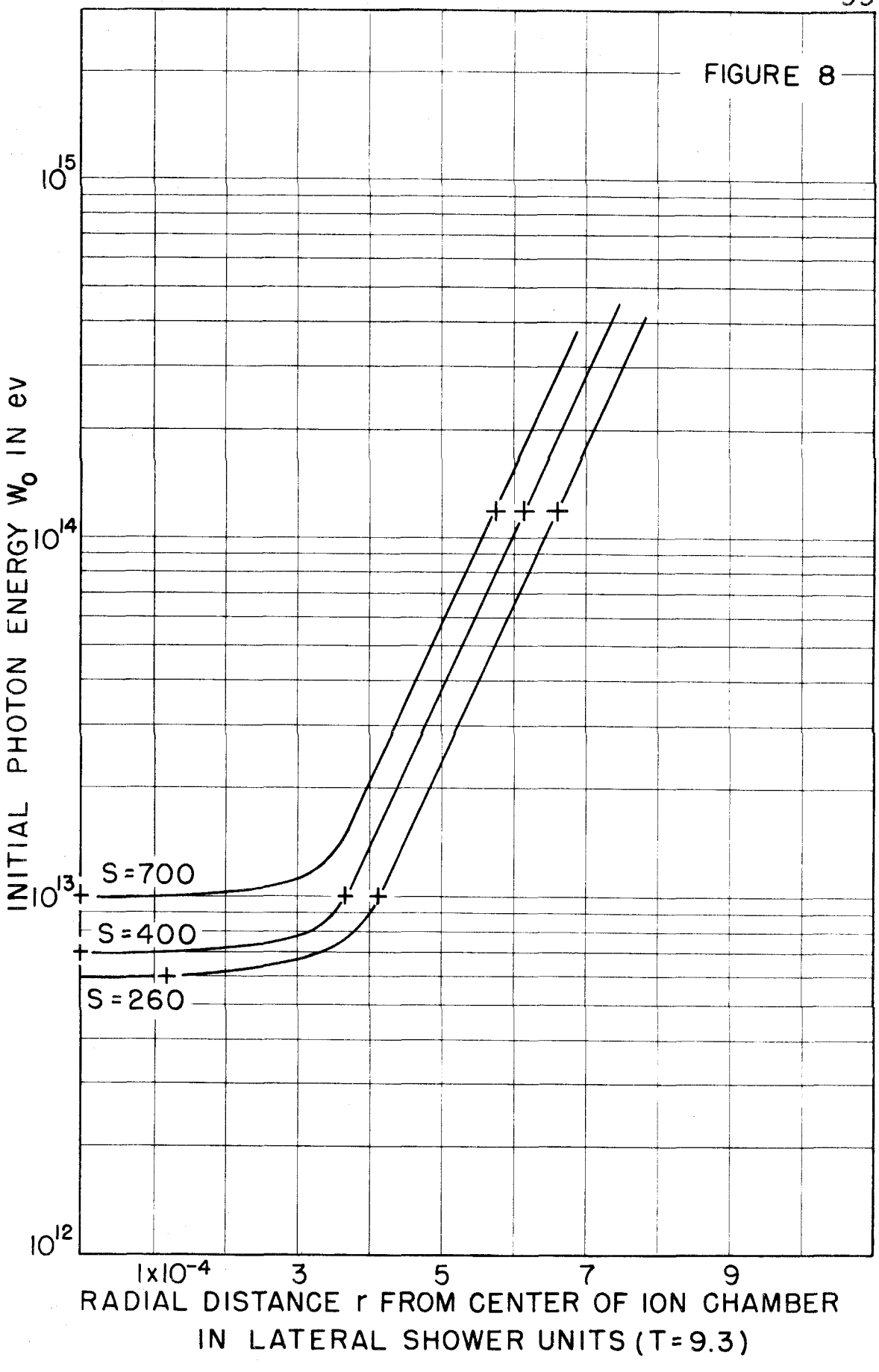
INITIAL PHOTON ENERGY W_0 IN ev
10^{15}
10^{14}
10^{13}
10^{12}
S=700
S=400
S=260
1x10^{-4}
3
5
7
9
RADIAL DISTANCE r FROM CENTER OF ION CHAMBER
IN LATERAL SHOWER UNITS (T=9.3)

FIGURE 9

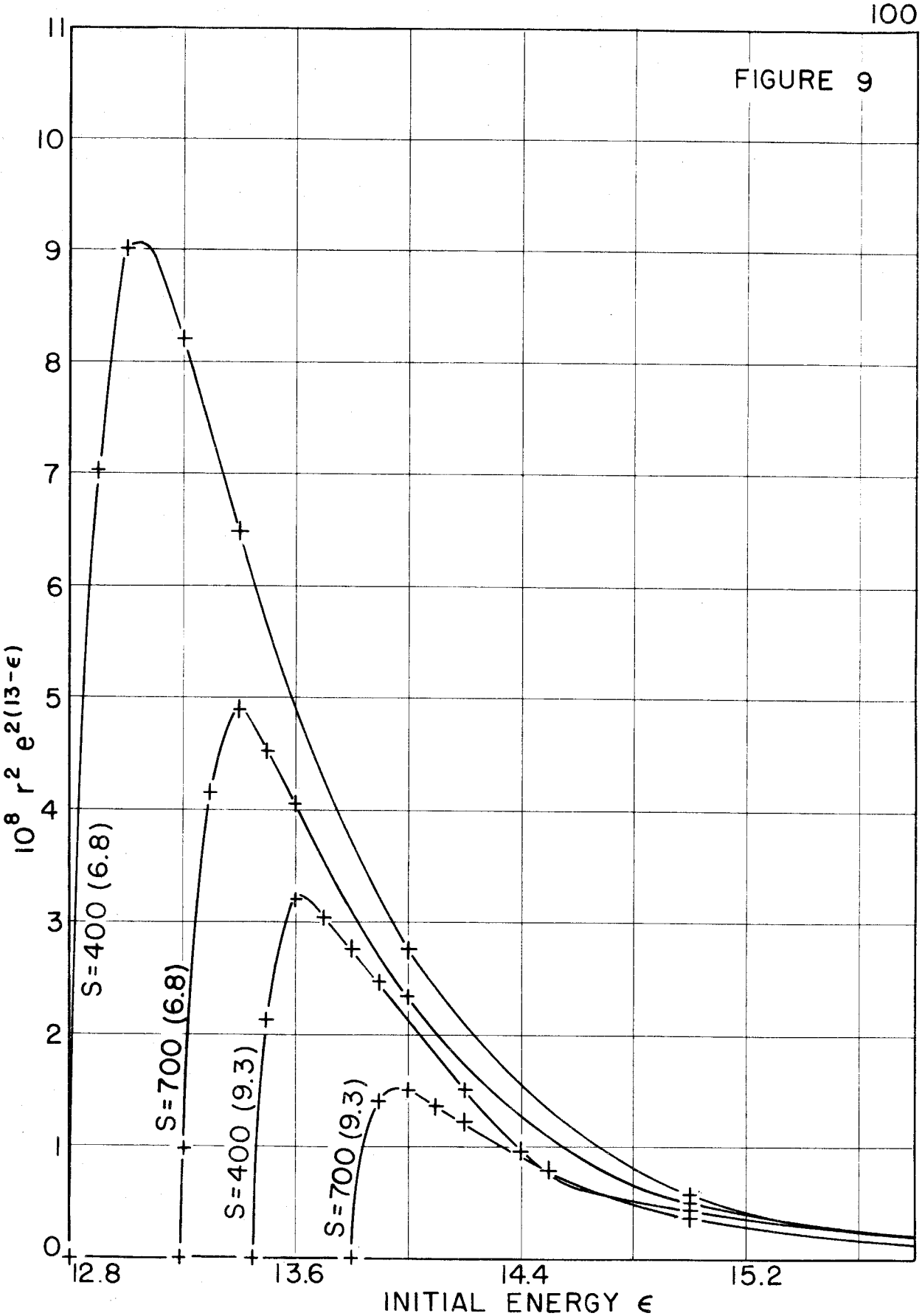
11
10
9
8
7
6
5
4
3
2
1
0
$10^8 r^2 e^{2(13-\epsilon)}$
S=400 (6.8)
S=700 (6.8)
S=400 (9.3)
S=700 (9.3)
12.8
13.6
14.4
15.2
INITIAL ENERGY ϵ

FIGURE 10

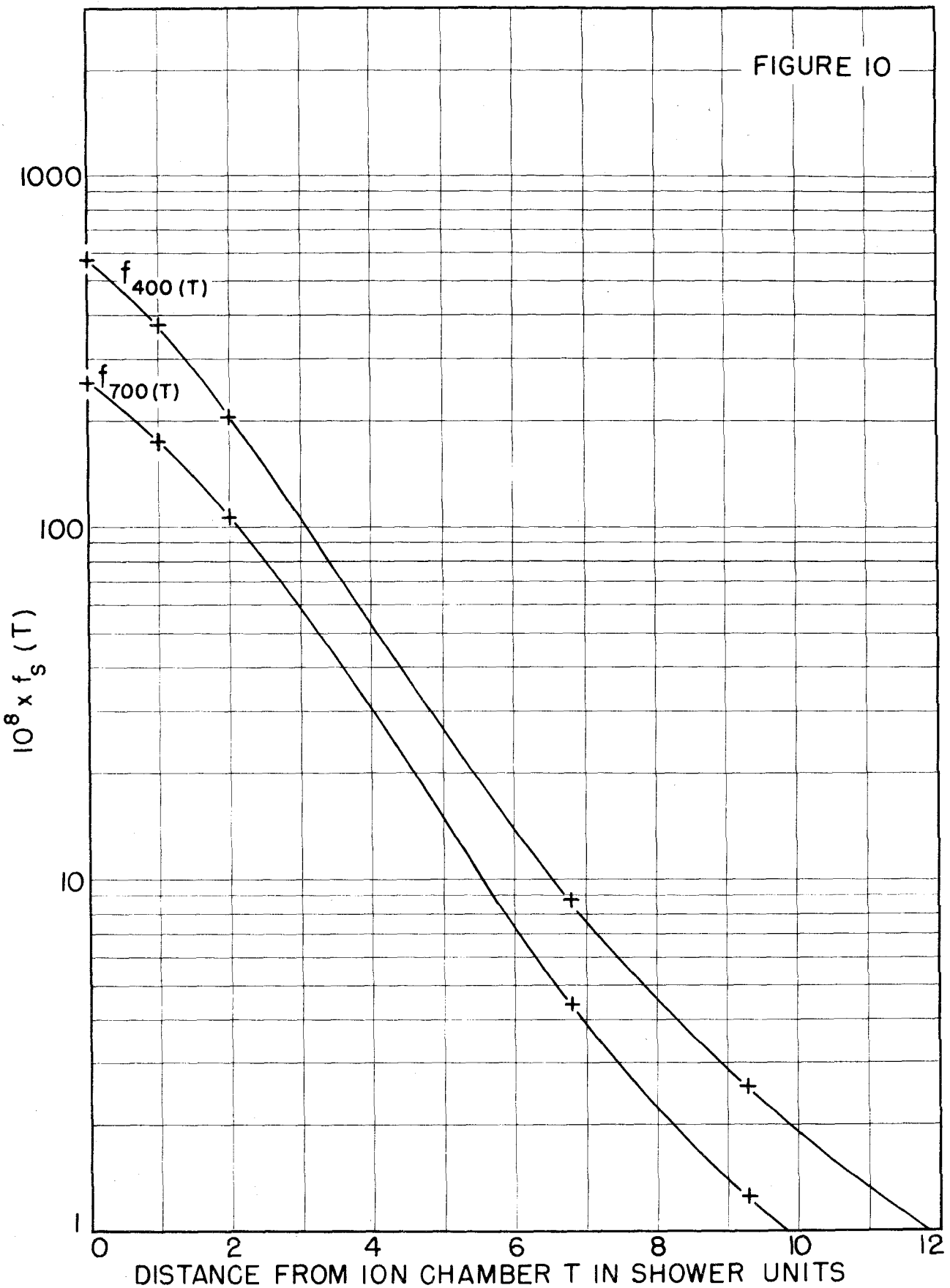
1000
100
10
1
$10^8 \times f_s(T)$
$f_{400}(T)$
$f_{700}(T)$
0
2
4
6
8
10
12
DISTANCE FROM ION CHAMBER T IN SHOWER UNITS

FIGURE 11

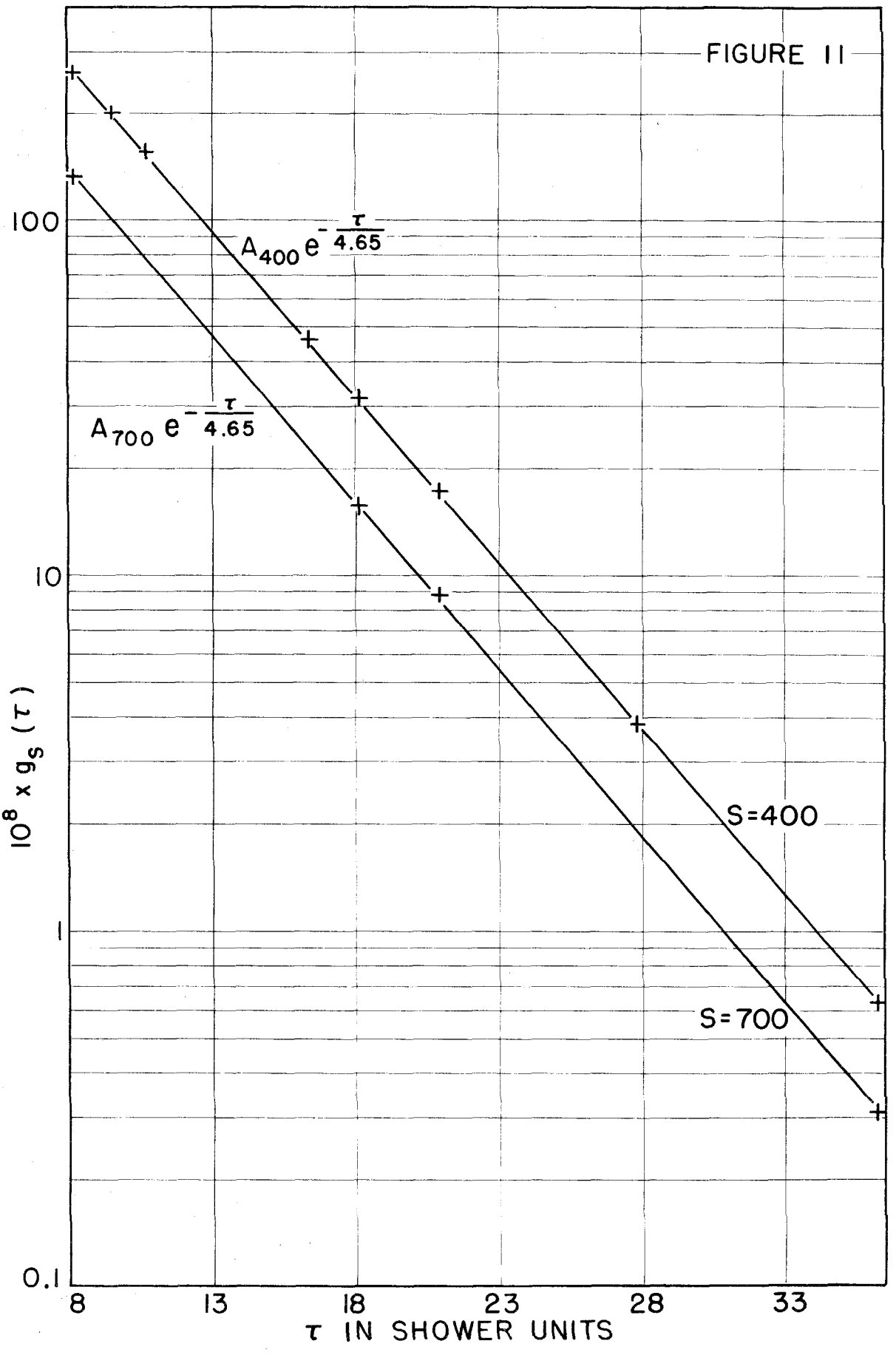
100
10
1
0.1
$10^8 \times g_s(\tau)$
$A_{400}\, e^{-\frac{\tau}{4.65}}$
$A_{700}\, e^{-\frac{\tau}{4.65}}$
S=400
S=700
8
13
18
23
28
33
τ IN SHOWER UNITS

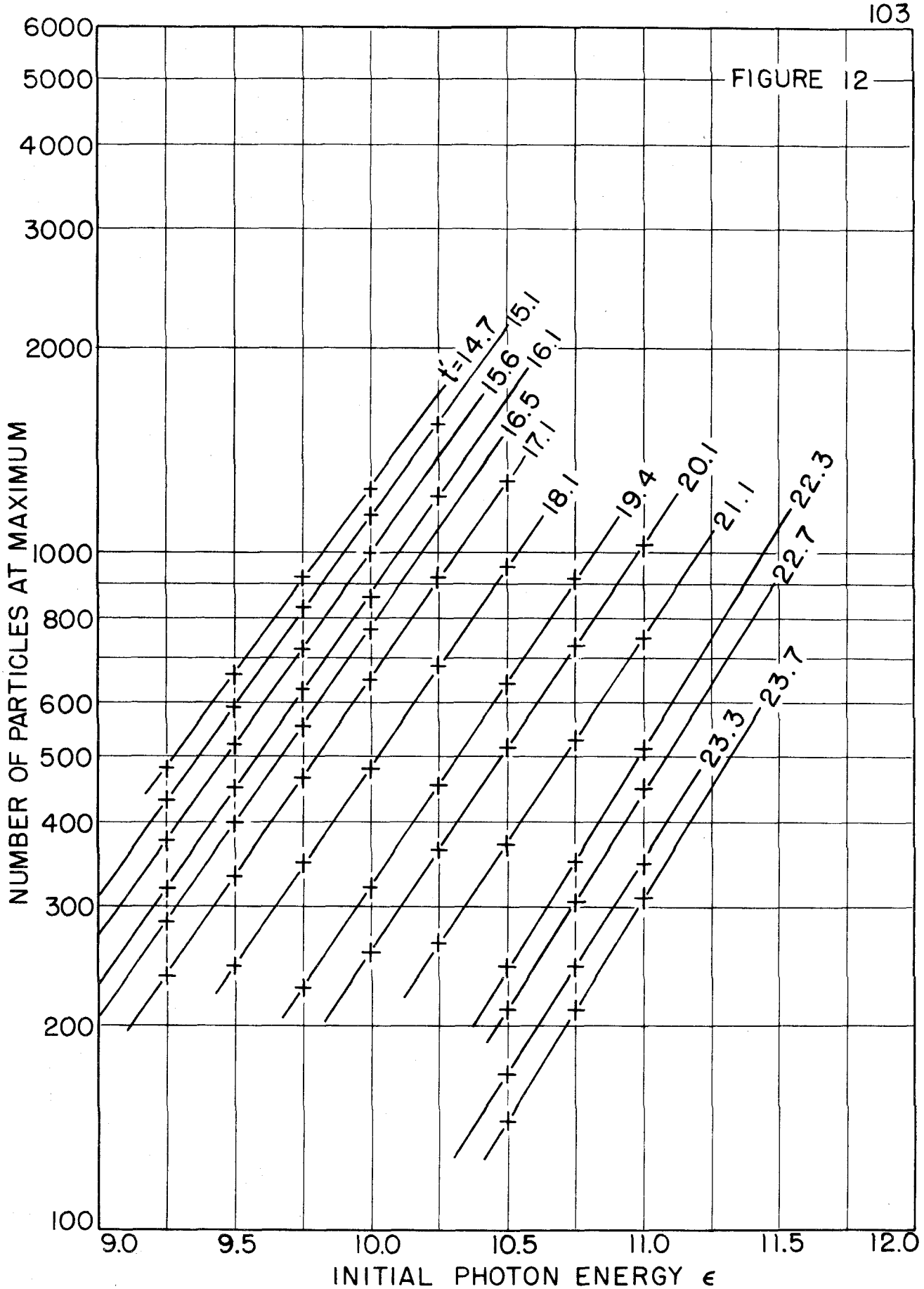
FIGURE 12
NUMBER OF PARTICLES AT MAXIMUM
INITIAL PHOTON ENERGY ϵ
6000
5000
4000
3000
2000
1000
800
600
500
400
300
200
100
9.0
9.5
10.0
10.5
11.0
11.5
12.0
t'=14.7
15.1
15.6
16.1
16.5
17.1
18.1
19.4
20.1
21.1
22.3
22.7
23.3
23.7

FIGURE 13

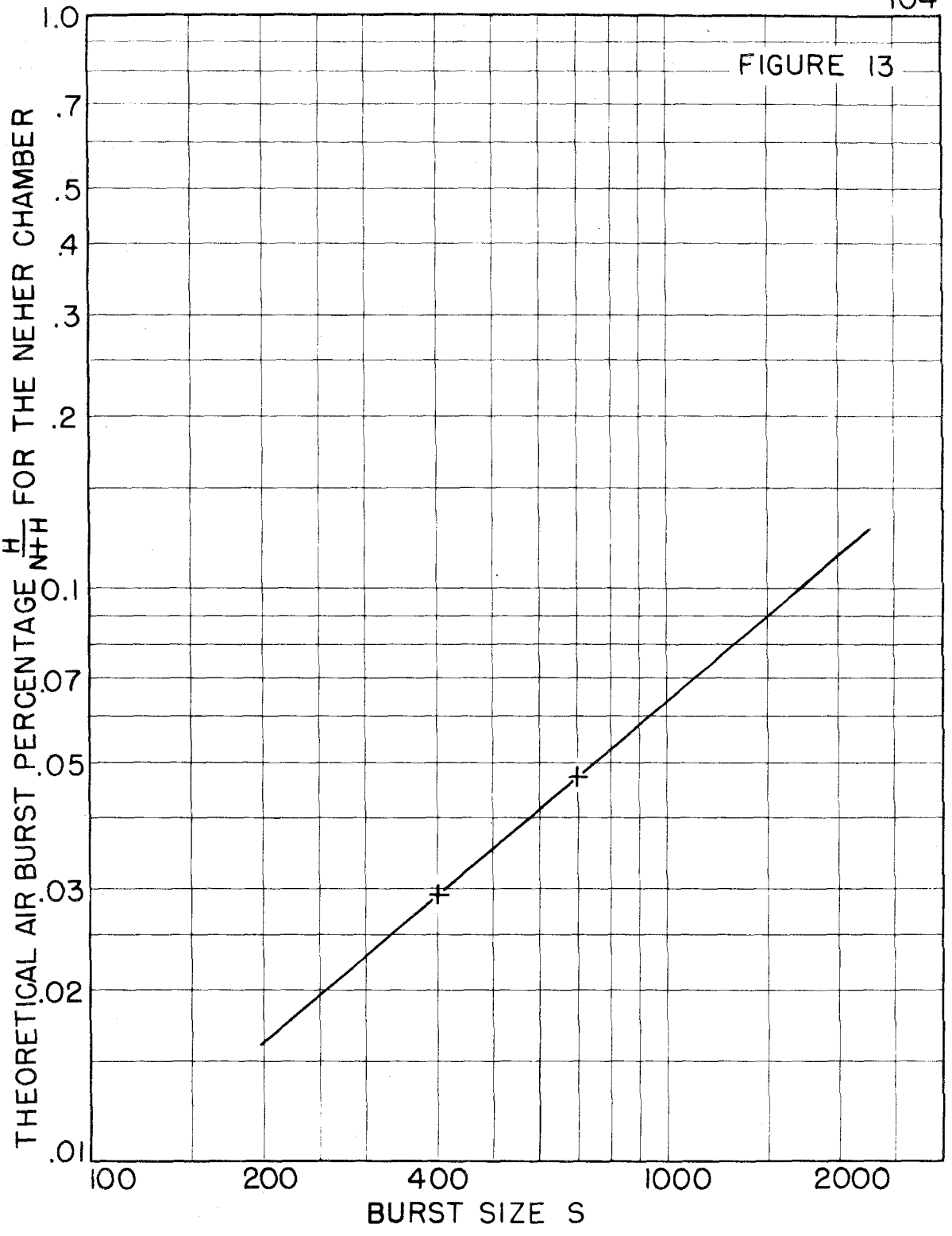
THEORETICAL AIR BURST PERCENTAGE $\frac{H}{N+H}$ FOR THE NEHER CHAMBER
1.0
.7
.5
.4
.3
.2
0.1
.07
.05
.03
.02
.01
100
200
400
1000
2000
BURST SIZE S

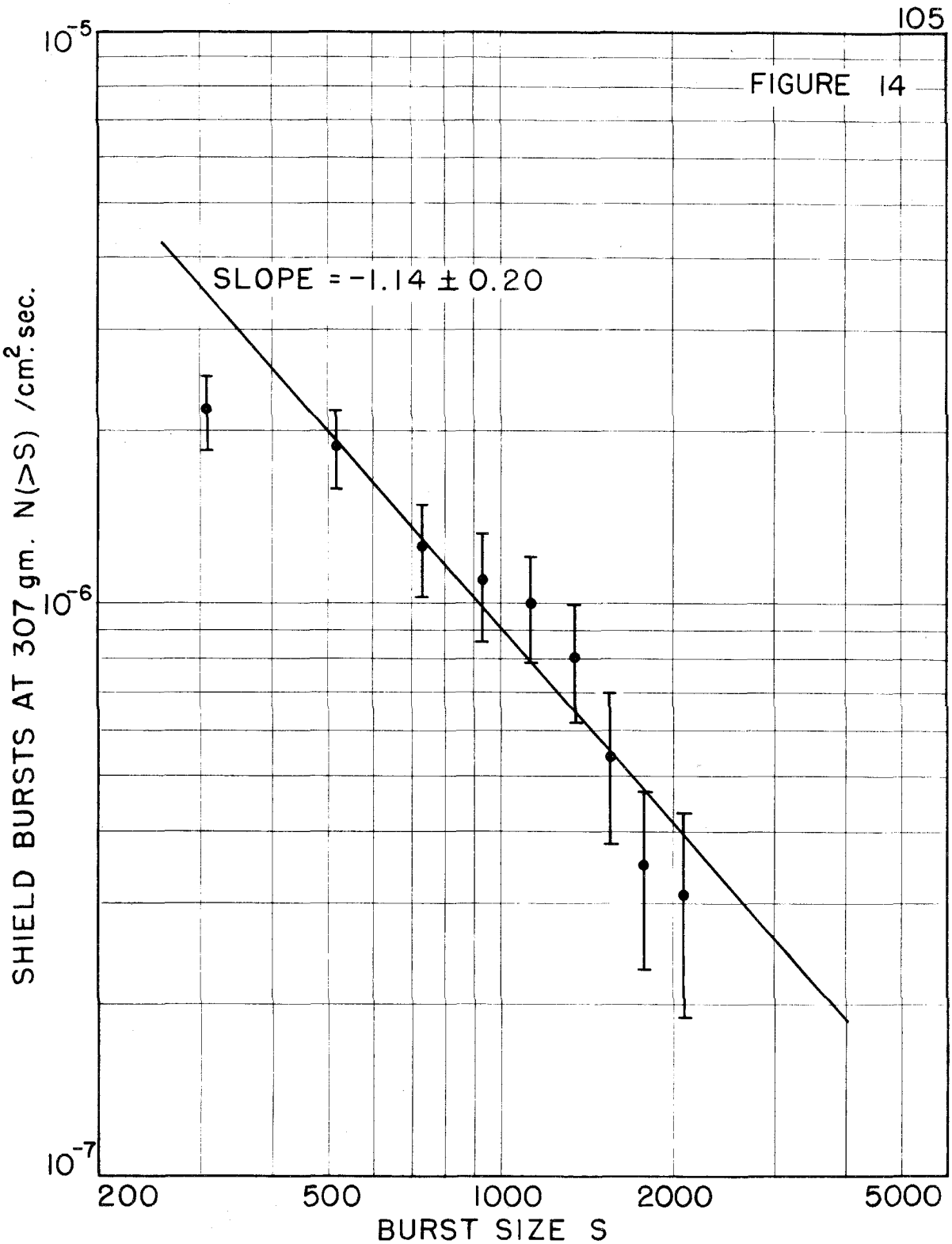
FIGURE 14
SLOPE = −1.14 ± 0.20
SHIELD BURSTS AT 307 gm. N(>S) /cm².sec.
10⁻⁵
10⁻⁶
10⁻⁷
200
500
1000
2000
5000
BURST SIZE S

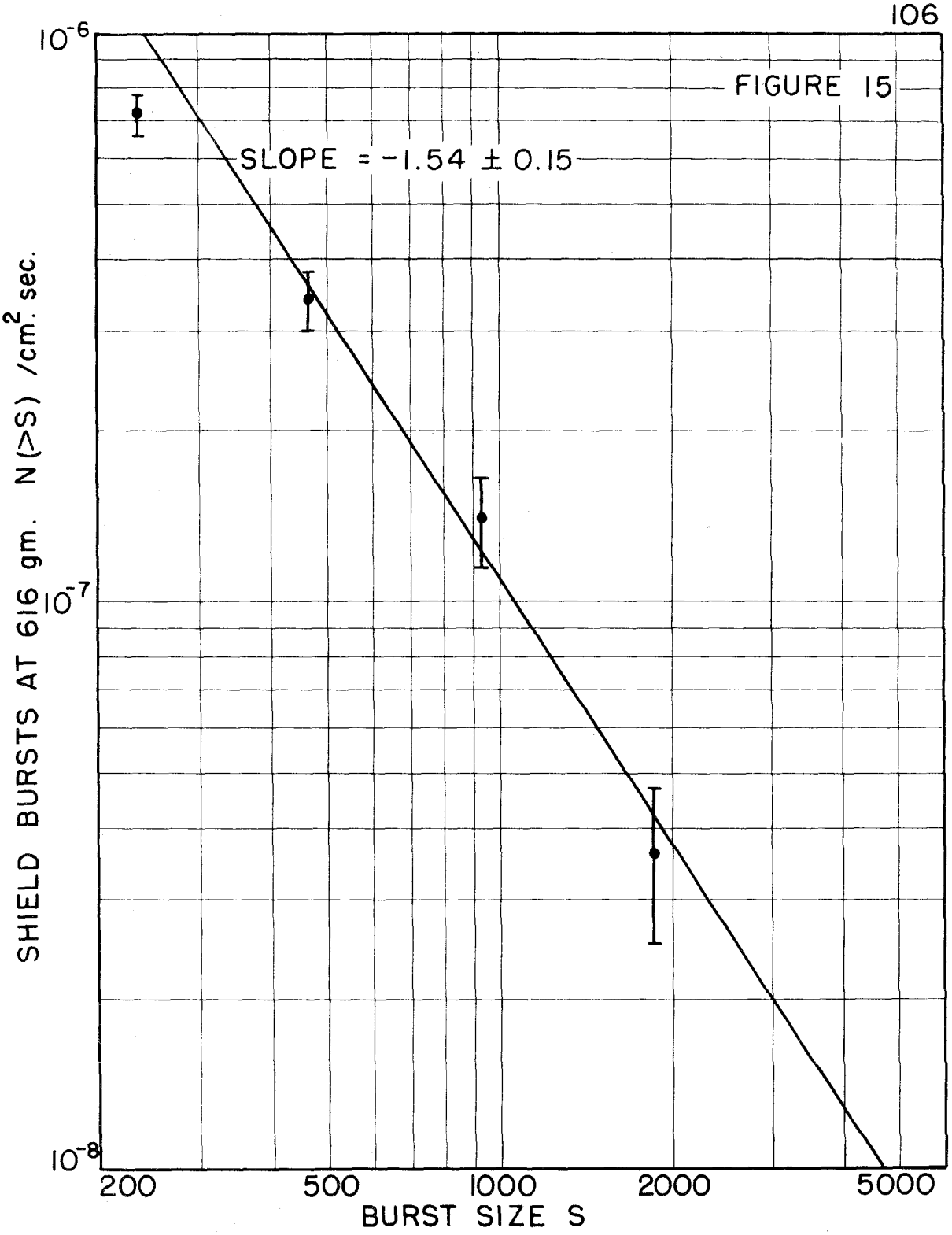
FIGURE 15
SLOPE = −1.54 ± 0.15
SHIELD BURSTS AT 616 gm. N(>S) /cm². sec.
10⁻⁶
10⁻⁷
10⁻⁸
200
500
1000
2000
5000
BURST SIZE S

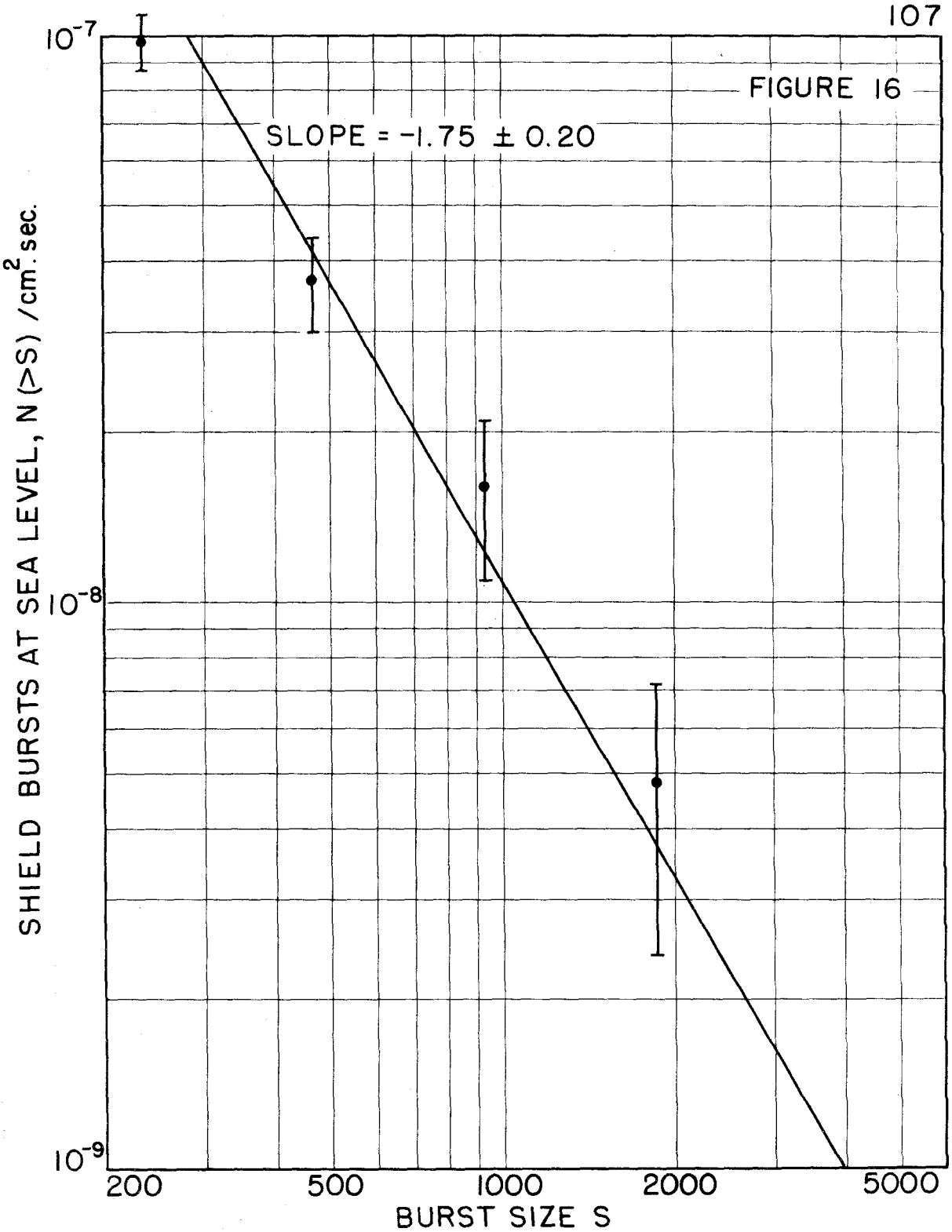
FIGURE 16
SLOPE = -1.75 ± 0.20
SHIELD BURSTS AT SEA LEVEL, N (>S) /cm².sec.
10⁻⁷
10⁻⁸
10⁻⁹
200
500
1000
2000
5000
BURST SIZE S

FIGURE 17

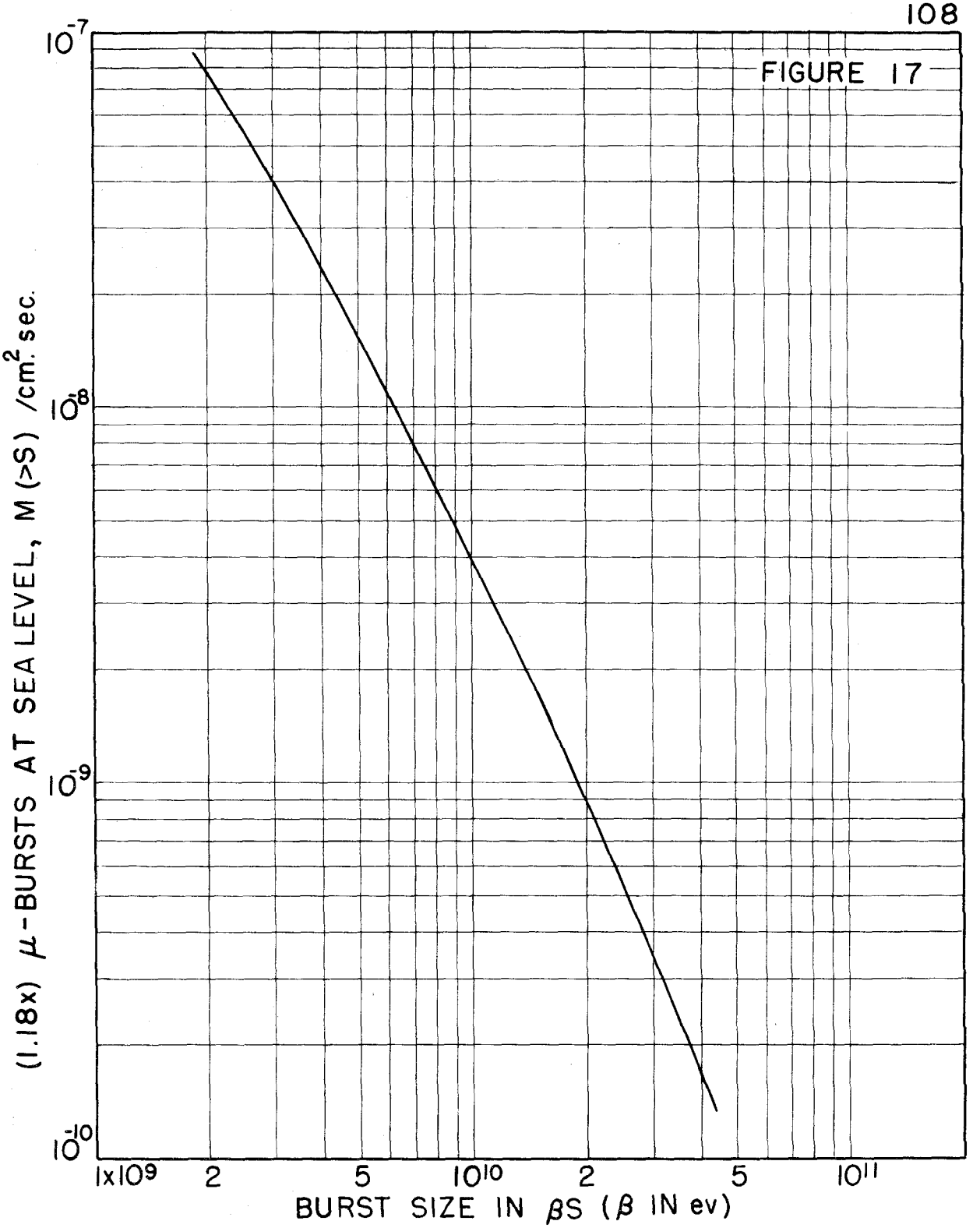
10^{-7}
10^{-8}
10^{-9}
10^{-10}
(1.18x) μ-BURSTS AT SEA LEVEL, M(>S) /cm.^{2} sec.
1x10^9
2
5
10^{10}
2
5
10^{11}
BURST SIZE IN βS (β IN ev)

FIGURE 18

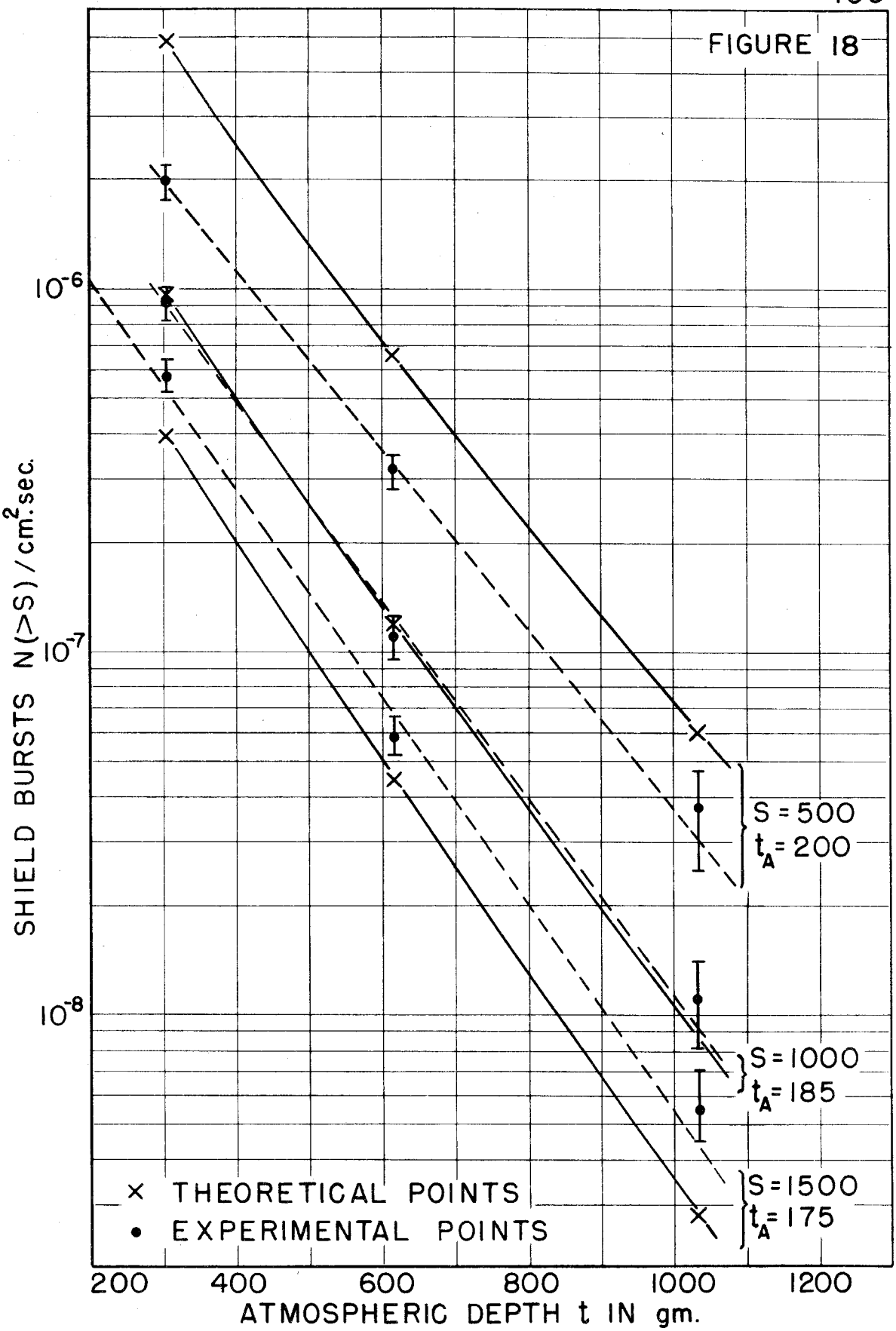
SHIELD BURSTS N(>S) / cm².sec.
10⁻⁶
10⁻⁷
10⁻⁸
S = 500
t_A = 200
S = 1000
t_A = 185
S = 1500
t_A = 175
× THEORETICAL POINTS
• EXPERIMENTAL POINTS
200
400
600
800
1000
1200
ATMOSPHERIC DEPTH t IN gm.

FIGURE 19